A DISPERSIONLESS TRANSMISSION GRATING BASED MICHELSON INTERFEROMETER FOR THE CHARACTERIZATION OF HARMONICS

By

Goulielmakis Eleftherios

MASTER'S THESIS

Supervisor: Prof. D. Charalambidis

PHYSICS DEPARTMENT-UNIVERSITY OF CRETE

POSTGRADUATE PROGRAM OF MICROELECTRONICS-OPTOELECTRONICS

HERAKLION, CRETE

SEPTEMBER 2002

Publications

1) E. Goulielmakis, G. Nersisyan, N. A. Papadogiannis, D. Charalambidis, G.D. Tsakiris, K. Witte *A dispersionless Michelson interferometer for the characterization of attosecond pulses.* Appl. Phys B **74**, 3, 197-206, (2002)

2) N. A. Papadogiannis, G.Nersisyan, E. Goulielmakis, T. P. Rakitzis, E. Hertz, D. Charalambidis G.D. Tsakiris, K. Witte, *Temporal characterization of short pulse third-harmonic generation in an atomic gas by a transmission grating interferometer.* Opt. Lett. **27**, 1561, (2002)

3) D. Charalambidis, N.A. Papadogiannis, E. Goulielmakis, G. Nersysian, G. D. Tsakiris and K. Witte, *A transmission grating interferometer for the temporal characterization of harmonics.* Journal of Modern Optics (In press)

Conference and network meetings presentations

1 E. Goulielmakis, G. Nersysian, N. A. Papadogiannis, D.Charalambidis, G. D. Tsakiris. *"Modelling of an XUV autocorrelator based on a transmission grating"* Atto network meeting 25-27 January 2001, Amphitheatre Francis Perrin Laboratoire de Chimie -Physique 11, rue Pierre et Marie Curie 75005 PARIS.

2 E. Goulielmakis, G. Nersisyan, N.A. Papadogiannis, and D. Charalambidis G.D. Tsakiris, K. Witte. *"A transmission grating based interferometer for the characterization of attosecond pulses"* Atto network meeting 20-23 November 2001, Polytechnico Di Milano.

3 E. Hertz, N.A. Papadogiannis, E. Goulielmakis, C. Kalpouzos, T.P. Rakitzis, G. Nersisyan, D. Charalambidis, G. Tsakiris, K. Witte. *"A dispersionless interferometer for the temporal characterization of harmonics and harmonic superpositions"* Third Annual Meeting of EU-Network COCOMO Sofia, Bulgaria, April 4-8, 2002.

4 N.A. Papadogiannis, E. Goulielmakis, G. Nersysian, D. Charalambidis, G Tsakiris, K. Witte. *"A transmission grating interferometer for the temporal characterization of harmonics"*, (Poster Session) 34^{th} Egas Sofia 9-12 July 2002, Europhysics Conference.

5 N.A. Papadogiannis, G. Nersisyan, E. Goulielmakis, E. Hertz, L. A. A. Nikolopoulos, T. P. Rakitzis, D. Charalambidis, G. D. Tsakiris, P. Tzallas, K. Witte,*"Attosecond Science: Present Status and Prospects"* , The XIV International Symposium On Gas Flow & Chemical Lasers and High Power Laser Conference, 26-30 August 2002,Wroclaw, Poland (Invited)

Table of Contents

List of Tables

List of Figures

Abstract

A new Michelson type interferometer, based on a transmission grating beam splitter, is presented and studied in detail. It posses dispersionless characteristics and flat spectral response, over the UV- XUV spectral range. Three variant configurations of the interferometer are examined, using ray tracing techniques. It was found that when certain imaging conditions are preserved, the interferometer exhibits extremely low dispersion and therefore its applicable for the temporal characterization of harmonics, and harmonic superpositions. Further, the interferometer is experimentally employed for the temporal characterization, of the third harmonic of a Ti:Saph laser. The results obtained, are coincide with those acquired with a conventional Michelson interferometer, as well as with the general conclusions of the ray tracing calculations.

Introduction

The rapid development of ultrashort high intensity laser pulses over the last decade, made possible the study of the interaction of strong electromagnetic fields with matter. High harmonics are generated, when atoms are exposed to strong electromagnetic laser fields, and experimentally this is achieved when an ultrashort pulse is focused in a gas medium. Today's laser technology, allows generation of harmonics of extremely high orders, reaching the XUV and soft x-rays up to the so called "water window" (Spielmann et al, 1999). The systematic study of the phenomenon is of great importance, not only because the harmonics provide a principal probe of understanding the nature of strong interactions between light and matter, but also because they possess special spectral and temporal characteristics for the implementation of table top XUV sources, of short pulse duration and high intensity, proper for further spectroscopical studies of atoms and molecules. Additionally, high harmonics have been proposed in the past (Farkas et al., 1990), as the most promising spectral source for the generation of XUV attosecond pulses.

Albeit a systematic metrology has been developed during the last decade for characterizing short pulses even of a few fs duration, attosecond measuring techniques have very recently appeared (Papadogiannis *et al.* 1999; Paul *et al.*, 2001; Hentshel *et al.*, 2001). However detailed studies for short duration harmonics and attosecond pulses, would require special XUV optics of extremely low dispersion and sophisticated designed apparatus, for their characterization. The design, the analysis and the experimental test of such apparatuses, is the subject of this thesis.

Outline of the thesis

The outline of this thesis is as follows: In *Chapter I*, an introduction to the fundamental pulse metrology principles will be given. It will be focused to the autocorrelation techniques, since they are mostly connected with this work. In the second part of the chapter, a short outline to the harmonic generation,the temporal and spectral characteristics of harmonics, as well as the way that they are involved in the generation of attosecond pulses, will be discussed. In *Chapter II*, a new type of an interferometer appropriate for the characterization of harmonics and attosecond pulses as well, will be presented. The ideas will be discussed in detail and will be confirmed by ray tracing calculations, in three different configurations of the setup proposed. Further in *Chapter III*, the interferometer, will be tested in the UV by its utilization for the temporal characterization of the third harmonic of a Ti:Saph laser. Finally, the thesis will complete, with general conclusions on the analyzed and experimentally tested interferometer.

Chapter 1

Pulse optics and harmonic generation

1.1 Introduction

This chapter comprises an outline to the fundamental concepts of the pulse optics, the pulse propagation to a medium and the metrology approaches that the last years have been developed for the characterization of short laser light pulses. Albeit, several techniques have been developed up today specially for the characterization of femtosecond pulses, only the autocorrelation techniques will be discussed here since they are mostly connected with the work presented in this thesis. Further, the fundamental principles of the high harmonic generation phenomenon and the generation of attosecond light pulses as a result of harmonic superposition, will be also outlined.

1.2 Pulse optics

1.2.1 Electromagnetic description of a pulse

Time frequency representation

The electric field of a linearly polarized monochromatic wave is described as:

$$E = Re(E_0 e^{i\omega_0 t})\widehat{y} \tag{1.1}$$

In order to describe a pulse, the above equation is multiplied by a bell shaped function. The simplest form is a gaussian function, constructing a so called "Gaussian pulse"

which can be written as:

$$E = Re(E_0 e^{-\Gamma t^2 + i\omega_0 t})\widehat{y} \tag{1.2}$$

The fourier transform of a gaussian pulse, is also a gaussian function which implies that the spectral components of a gaussian pulse, will follow a gaussian distribution around the principal frequency ω_0 of the pulse. Since time and spectrum are related, there is always an "uncertainty" relation, connecting the spectral width around the central frequency ω_0 and the duration of the pulse. Generally, one can prove that this relation is pulse shape depended and for the case of a gaussian pulse has the form:

$$\Delta t \Delta\omega \geqslant \frac{1}{2} \tag{1.3}$$

When the equality holds, the pulse is said to be Fourier transform limited and obviously its duration is the minimum that can be achieved with the given spectral bandwidth. For different pulse shapes, there is also a corresponding relation between pulse duration and bandwidth, having the general form: $\Delta t \Delta\nu = K$. Typical values of K for various pulse shapes are given in table 1.2.1.

Shape	$f(t)$	$\Delta t \Delta\nu = K$
Gaussian	$exp(-(t/t_0)^2/2)$	0.441
Rectangle	-	0.892
Lorentzian	$[1 + (t/t_0)^2]^{-1}$	0.142

Table 1.1: Values for K, for various pulse shapes.

When a light pulse travels through a medium, the component frequencies are separated in time, due to wavelength depended index of refraction that it posses. There are two main effects corresponding to the pulse propagation on the material. The first one is that the pulse center is temporally delayed with respect to a replica of the pulse, that would travel equal geometrical distance, in vacuum. The second effect, is that the higher frequencies are usually (far from resonances) delayed with respect to the lower frequencies. The material is then said to have positive dispersion,

and the pulse is known to become positively chirped. This temporal redistribution of the spectral components is resulting to a pulse broadening. In order to formulate these ideas in a quantitative way, a mathematical description is necessary. Assume that $\varphi(\omega)$ is the phase spectral distribution of the pulse. The phase can always be expanded to a Taylor series around the central frequency of the of the pulse ω_0.

$$\varphi(\omega) = \varphi(\omega_0) + (\omega - \omega_0)\varphi^{'}(\omega_0) + \frac{1}{2}(\omega - \omega_0)^2\varphi^{''}(\omega_0) + \frac{1}{6}(\omega - \omega_0)^3\varphi^{'''}(\omega_0) + ... \quad (1.4)$$

where $\varphi^{'}(\omega)$ is the group delay (GD) $\varphi^{''}(\omega)$ the group delay dispersion (GDD) and $\varphi^{'''}(\omega)$, $\varphi^{''''}(\omega)$ the third and forth order dispersion respectively. GD and GDD are most commonly used, in order to characterize the dispersion characteristics of a medium, except when higher orders have to be considered. In order to connect GDD with the temporal broadening of a pulse travelling through a dispersive medium, lets consider a pulse of central carrier frequency ω_0 and duration τ_{in} defined at the FWHM. The electric field will have the form:

$$E_{in} = E_0 exp\left[-\left(\frac{2ln2t^2}{\tau_{in}^2}\right) + i\omega_0 t\right] \quad (1.5)$$

If we assume only a GDD term contribution when the above pulse is travelling through a medium, at the end of the medium the electric field of the final pulse will be (Siegman, 1960):

$$E_{in} = E_0 exp\left[(i\omega_0 t - \varphi) - \Gamma(t - \varphi')\right] \quad (1.6)$$

where Γ is related with the GDD as:

$$\Gamma = \left(\frac{\tau_{in}^2}{2ln2} + 2i\varphi^{"}\right)^{-1} \quad (1.7)$$

Finally the initial and the final pulse duration are related as:

$$\frac{\tau_{out}}{\tau_{in}} = \sqrt{1 + \frac{\varphi^{"2}}{\tau_{in}^4} 16\ln 2} \quad (1.8)$$

Since (GDD) is a known parameter for an optical system, equation (1.8) allows a direct estimation of the pulse broadening, which could be important only if $\varphi^{"} \geq \tau_{in}^2$. Finally the GDD can be directly expressed, as a function of the index of refraction, for a specific medium. If λ_0 is the central wavelength and l the medium length then:

$$\varphi^{"} = \frac{{\lambda_0}^3 l}{2\pi c^2} \frac{d^2 n(\lambda)}{d\lambda^2} \tag{1.9}$$

Thus $\varphi^{"}$ can be obtained for a medium if the dependance of the index of refraction $n(\lambda)$ as a function of the wavelength is known.

1.2.2 Pulse metrology

Autocorrelation techniques

In recent years, several techniques have been developed for the temporal characterization of short laser pulses. Unfortunately, techniques involving direct pulse measurement are limited by the response of the detectors, which cannot be less than a few nanoseconds so far. From the other hand, picosecond pulses or a minimum of a few hundreds of femtosecond, is the limit of semidirect techniques like streak cameras.

An alternative way for measuring the pulse duration of even shorter pulses, is the correlation method. Assume two time depended functions $F(t)$ and $F'(t')$. The first order correlation function $G(\tau)$ is defined as:

$$G(\tau) = \int_{-\infty}^{+\infty} F'(t) F(t-\tau) dt \tag{1.10}$$

If one of the $F(t)$ and $F'(t')$ is known the other one can be determined by the deconvolution of the $G(\tau)$. when ultrashort pulses have to be characterized, the test function is difficult to be synthesized, and a replica of the pulse is used as the probe. In this case we speak about the so called autocorrelation functions. Autocorrelation functions can be connected with the interferometric intensity output of an interferometer. The principle of a Michelson interferometer is depicted in Fig.1.1. The initial pulse is split in two replicas and the delay between the two replicated pulses,

is introduced by varying the position of the mirrors M1 or M2. The Interferometric output registered by a detector as a function of the delay introduced between $E(t)$ and $E(t-\tau)$, is expressed as:

$$I_1(\tau) = \int_{-\infty}^{\infty} |E(t) + E(t-\tau)|^2 dt \tag{1.11}$$

which is connected with the first order autocorrelation function as:

$$I_1(\tau) \propto 2 \int I(t)dt + 2G(\tau) \tag{1.12}$$

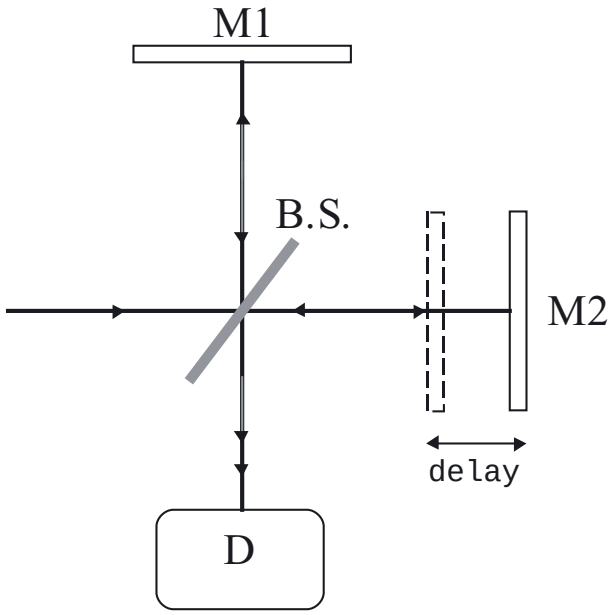

Figure 1.1: Basic principle of a Michelson type optical correlation. M1, M2 mirrors, B.S. beam splitter, D detection unit.

According to the theory of optical coherence, the electric field evolution of a pulse can be fully revealed, if all the nth order autocorrelation functions $G(\tau)^n$, are known. Of course this would require an infinite number of functions, in order for the optical pulse to be fully characterized. It can be shown that the knowledge of the second order of autocorrelation function $G(\tau)^2$ is sufficient, if one assumes that the pulse envelope has a reasonable shape i.e. gaussian, $Sech^2$ e.t.c. The second order autocorrelation

function can be expressed as:

$$I_2(\tau) = \int_{-\infty}^{\infty} \left||E(t) + E(t-\tau)|^2\right|^2 dt \tag{1.13}$$

All the above functions can be mimicked, using multiphoton processes. These processes require a special detection unit, with nonlinear intensity response. For the case of infrared femtosecond pulses, generation of the second harmonic on a BBO crystal, or a specially designed semiconductor based diode, with nonlinear response, may play the role of the proper detection unit.

Interferometric Autocorrelation

In Fig.1.2.a a calculated first order and in Fig.1.2.b a second order interferometric autocorrelation trace are depicted. These plots are based on the equations (1.12) and (1.13) respectively assuming gaussian shaped pulses. This assumption is also critical for expanding equation (1.13) in an analytic form:

$$I_2(\tau) = 2 + [4 + 2\cos(2\omega\tau)\, exp[-1/2(\tau/\tau_p)^2] + 8\cos(\omega\tau)\, exp[-(3/8)(\tau/\tau_p)^2] \tag{1.14}$$

where τ_p is the pulse duration τ the introduced delay and ω the central frequency of the pulse. Evaluating equation (1.14) in the two limits for the delay $\tau \to 0$ and $\tau \to \infty$ it results that the peak to background ratio for the second order interferometric autocorrelation is 8:1 (see Fig.1.2.b). In order to experimentally perform an interferometric autocorrelation the delay introduced between the two branches of the interferometer has to sweep in much smaller temporal steps than the cycle period of the studied pulse. Once an experimental autocorrelation trace has been received, it can be fitted to an equation similar with (1.14) and the pulse duration τ_p can be extracted. if the experimental signal obtained posses low statistics, the fitting in to autocorrelation functions, is quite difficult. An alternative method, is the averaging of the interferometric trace in to a simpler curve. This can be performed either using

a numeric algorithm, or directly by interferometry measuring the so called intensity autocorrelation.

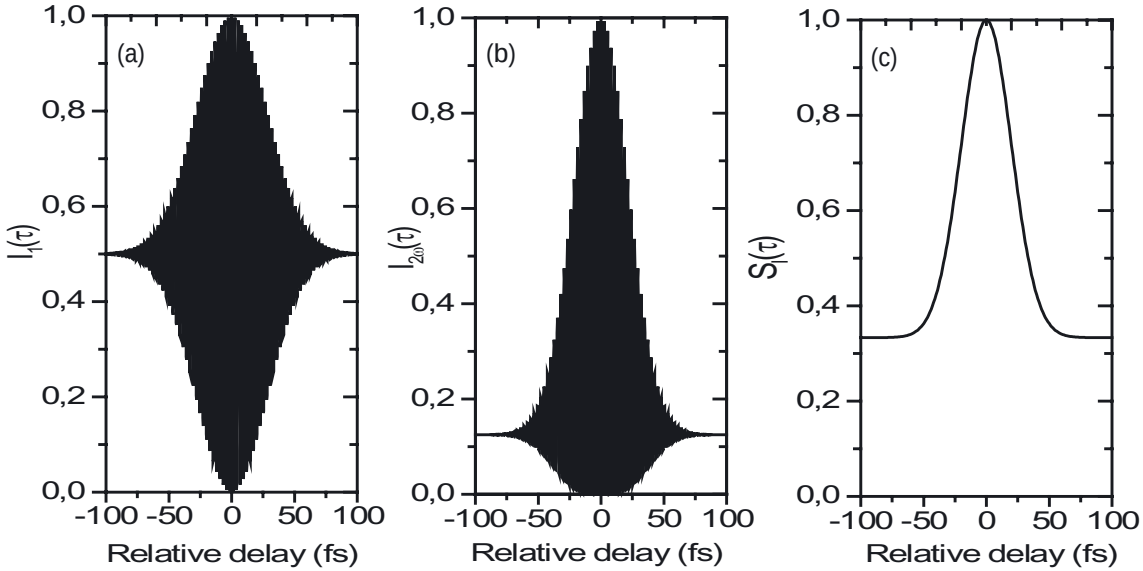

Figure 1.2: Theoretically produced autocorrelation traces: **a.** Single order interferometric autocorrelation. **b.** Second order interferometric autocorrelation. **c**. Intensity autocorrelation.

Intensity Autocorrelation

In the intensity autocorrelation the delay is swept quite fast (the delay step is bigger than the period of cycle of the pulse), in order to perform an action similar to that obtained by the numerical averaging. The signal in that case will have the form:

$$S_I = 2\int I^2 dt + 4\int I(t)I(t-\tau)dt \tag{1.15}$$

A theoretical trace of an intensity autocorrelation is shown in Fig.1.2.c. It can be easily, shown that the peak to background ratio is 3:1.

Real pulse duration

As mentioned previously, in order to calculate the duration of the original pulse, a reasonable pulse shape has to be assumed. Depending on that shape, the reveal of the original pulse duration differs. In Table 1.2.2, mathematical results concerning various commonly used pulse shape models are listed. In this table T corresponds to

Function	$x \equiv t/T$	τ_p/T	τ_G/T	τ_p/τ_G
Square	$\begin{cases}1;\|t\|\leq T/2\\0;\|t\|>T/2\end{cases}$	1	1	1
Diffraction function	$\frac{\sin^2(x)}{x^2}$	2.7831	3.7055	0.7511
Gaussian	e^{-x^2}	$2\sqrt{\ln 2}$	$2\sqrt{2\ln 2}$	0.7071
Hyperbolic Sech	$sech^2(x)$	1.7627	2.7196	0.6482
Lorentzian	$\frac{1}{(1+x^2)}$	2	4	0.5

Table 1.2: The relationship between pulsewidth τ_p and autocorrelation width τ_G, for various pulseshape models, commonly used in autocorrelation technics (Sala *et al.*, 1980).

the pulse duration of each function, τ_p to the FWHM pulse duration and τ_G to the autocorrelation pulse width.

1.3 Harmonic generation

High harmonics are generated when atoms are exposed to strong laser electromagnetic fields. A generic harmonic spectrum is depicted in Fig.1.3.a. It is consisted of a series of odd multiples of the fundamental radiation, exhibits a rapid decrease in the lower orders and a long extended plateau followed by a sharp cut-off. In Fig.1.3.b a calculated harmonic spectrum resulting from the one dimensional integration of the schrödinger equation is depicted (Goulielmakis, 2000). Several theoretical models have successfully explained the generic shape, and most of them are based on the so called 'three step model' proposed by Corkum and Co-workers (Corkum, 1993).

According to this model, when the atom is exposed to a strong laser field the electron motion can be described in three main steps:

- The electron tunnels into the continuum, through the suppressed by the electric field, potential barrier.
- Under the influence of the laser field, the electron acquires kinetic energy and when the field changes its sign, it may return to the core vicinity.
- Close to the core region, the electron has a finite possibility to recombine and to emit harmonic photons.

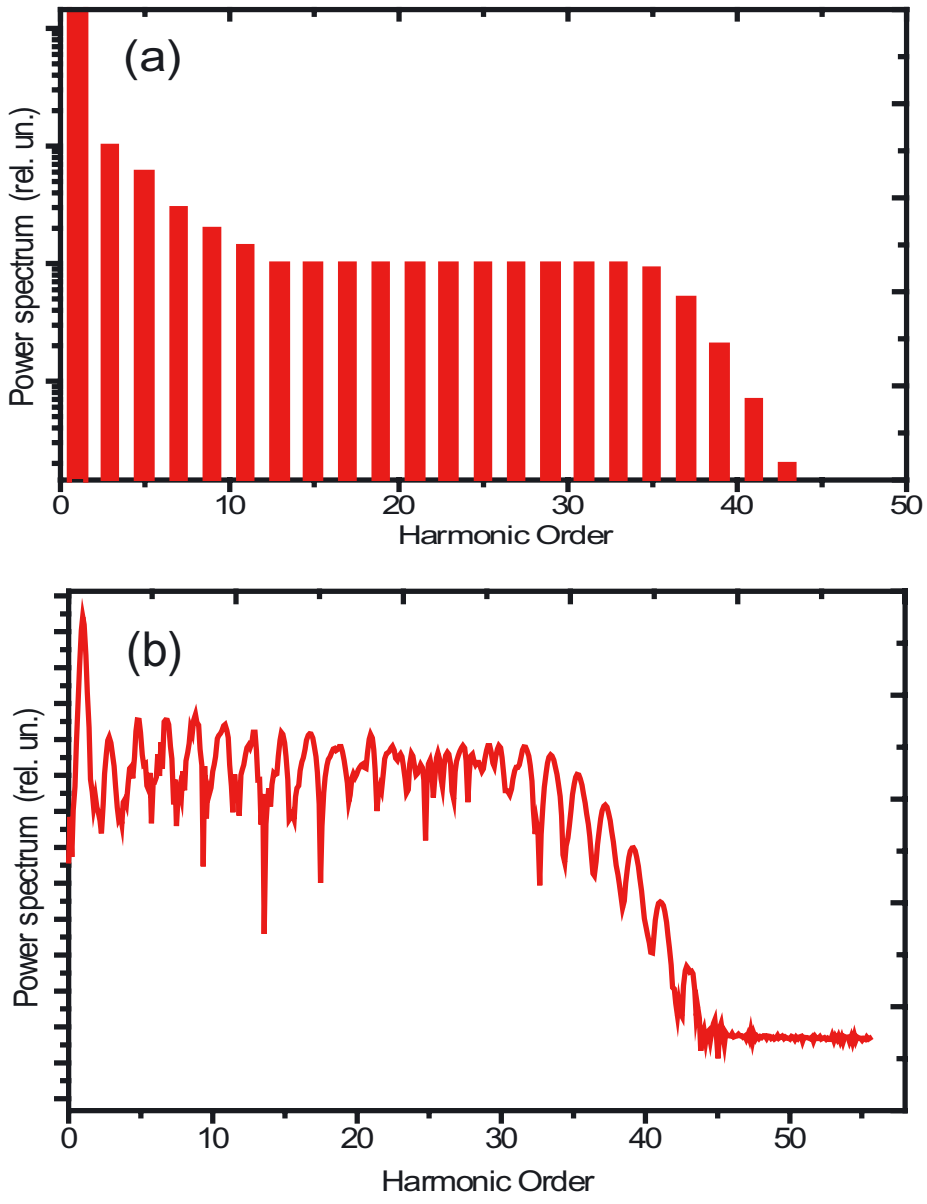

Figure 1.3: **a.** Generic harmonic spectrum. **b.** Calculated harmonic spectrum, using an 1-D integration of the Schrödinger equation.

From the above consideration it is clear that the harmonic photon emission is sensitive to the phase of the electric field. An electron ejected from the atom by the electric field, may return back and recombine, only if it is released to the continuum just after the peak of the electric field. In every other time of ejection, the electron never returns to the core vicinity and the atom is ionized. Since the electron is ejected far away from the core, it behaves as a classical particle and its motion can be successfully described by newtonian dynamics. Models based on these considerations, have successfully predicted that cut-off energy is given by:

$$E_{max} = I_p + 3.17U_p \tag{1.16}$$

where I_p denotes the ionization potential of the atom, and U_p is the ponteromotive energy, corresponding to the mean energy that the electron could acquire through its oscillating motion under the influence of the laser electric field. This rule has been experimentally confirmed by several experimental works (L'Huillier *et al.*, 1993; Macklin *et al.*, 1993; Papadogiannis *et al.* 1999) so far.

Albeit the effect of harmonic generation is quite well understood and several works have contributed to the optimization of the generation and to the development of high energy harmonic sources (Zhou *et al.*, 1996; Schnurer *et al.*, 1998; Constant *et al.*, 1999 ; Papadogiannis *et al.*, 2001) allowing further spectroscopical studies, their temporal characteristics are not well accessed yet. There are several reasons which contributed to that. On the one hand, the complete lack of materials proper for beam splitting, necessary for autocorrelation techniques of the harmonic radiation due to the high absorbability of matter in the UV-XUV region. On the other hand, in order to access the temporal characteristics of a harmonic pulse, the knowledge of the higher than the first order autocorrelation function is necessary, requiring nonlinear materials for detection at that spectral regime. Additionally, the XUV, is probably the most difficult spectral region for manipulation. The efficient filtering of desired part of the

spectrum requires special designed optics and filters which unfortunately, are proper only for very specific bands. Nevertheless interesting experiments, have investigated nonlinear processes involving harmonic pulses (Xenakis *et.al.*, 1996; Kobayashi *et al.*, 1998; Sekikawa *et al.*, 1999), or group of harmonics (Papadogiannis *et al.*, 2002) and have successfully detected second order processes in rare gasses.

An alternative way of accessing the temporal characteristics of a harmonic pulse, is the so called cross correlation methods. in these methods, the replica of the harmonic pulse is replaced by the fundamental and the necessary nonlinearity is induced due to its high intensity (Toma *et al.* 2000; Norin *et al.*, 2002). The resolution of a cross-correlation method, is strongly application depended. In the simplest form of a cross correlation method, the temporal resolution is limited by the probe pulse and therefore only harmonics broader than the fundamental could be characterized. In a more sophisticated form however, these methods can be possessed by much higher resolution, and can be extended even to the characterization of attosecond pulses localized in the high harmonic generation.

1.4 Attosecond pulses

It has been proposed (Farkas *et al.*,1990) that high harmonics could be properly entangled, in a similar manner that laser modes in a cavity are locked, in order to produce trains of attosecond pulses. The idea is illustrated in Fig.1.4. The frequency spacing between two neighbor "harmonic" modes, is twice the frequency of the fundamental ω. Therefore, selecting a reasonable number of harmonics lets say N, the pulse duration of the burst would be $T_{pulse} = T_{Laser}/2N$. For example, assuming a laser central wavelength of 800 nm and a selection of 5 harmonics from the plateau, the above formula results to $T_{pulse} = 266\ as$.

The previous estimations, assumed that harmonics are phase locked. However theoretical studies (Antoine *et al.*, 1996) have shown that when only the atomic response is considered, harmonics are not generally phase locked. If the phase of the

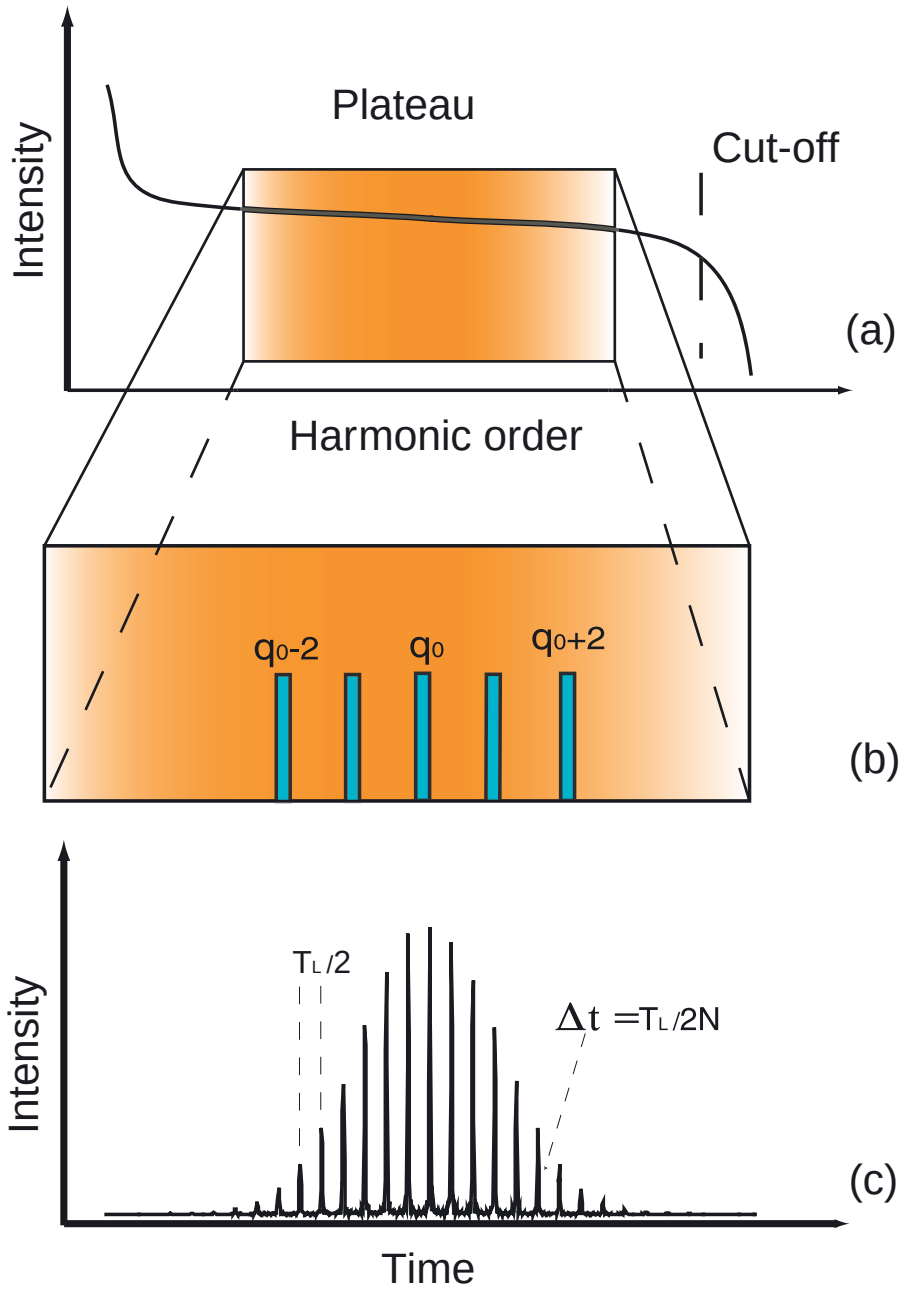

Figure 1.4: **a.** Filtering of an appropriate band of plateau harmonics. **b.** Expansion of this band. **c.** A train of attosecond pulses, resulting by their superposition.

selected harmonics is slightly different, this would result in more than two successive attosecond pulses, within the half period $T_{laser}/2$ of the fundamental. Nevertheless, harmonics propagation effects in the generation volume, have been reported to play a phase filtering role and finally two attosecond bursts per period may appear. A method of producing single pulses has been proposed by Corkum (Corkum *et al.*, 1994; Corkum, 1996) and it is based in the composition of two perpendicular polarized laser pulses, with slightly different central frequency, resulting to a temporal modulation of the ellipticity degree of the total pulse. Since high harmonics are efficiently generated only by linearly polarized laser light, the harmonic generation is limited within a fraction of a laser cycle, resulting to a single isolated attosecond burst. Additionally, calculations (Christov et al. 1997) have shown that when sub-ten femtosecond pulses are utilized, the generation of utra-high harmonics is limited only in a fraction of the pulse around its peak, resulting to single isolated pulses when a 10% of the total harmonic spectrum near the cut-off regime is selected.

Up to now strong indications of attosecond pulses trains localized in the HOHG have been reported (Papadogiannis *et. all.*, 1999, Paul *et al.*, 2000). Further a method for producing and measuring single, few hundreds attosecond pulses has been experimentally demonstrated (Drescher *et al.*, 2001, Hentschel *et al.*, 2001).

In the last three techniques mentioned, the laser fundamental is involved for accessing the temporal characteristics of the investigated pulses, using cross-correlation methods. This involvement, is either connected with the phase and amplitude information retrieval for every harmonic of the pulse (Paul *et al.*, 2000), or by inducing the necessary nonlinearity, providing a comparison between the XUV pulse with the fundamental (Drescher *et al.*, 2001, Hentschel *et al.*, 2001). Further investigation of harmonics or even more of attosecond pulses, would require the design of an experimental apparatus, providing low dispersion to the examined pulses, broadband operation in order to expand the study over the the UV-XUV spectral regime, high resolution of measurement, as well as the investigation of proper detection units,

providing the nonlinearity necessary for their accurate characterization.

Chapter 2

The Grating XUV Interferometer

2.1 From the conventional Michelson to the XUV grating interferometer

The idea of utilizing diffraction gratings in the laser interferometry, is rather old (Ronchi; 1963)and has been experimentally implemented for the development of various types of interferometers, proper for the characterization of CW lasers. However, the direct implementation of gratings for manipulating femtosecond pulses is rather difficult, because the dispersion introduced is strongly affecting their temporal characteristics. Nevertheless, the demand of optical devices allowing the control of femtosecond pulses, brought back again their utilization in combination with special designed optics, either for the construction of temporal stretching and compression units, for the development of high intensity ultrafast lasers, or for the design of spatial light modulators, allowing the generation of femtosecond pulses with accessible characteristics employed in modern coherent control experiments. The key point in all the previous examples, is the control of the introduced dispersion to the pulses under manipulation, which is achieved by proper optical configuration and imaging techniques. In what follows,the idea of grating beam splitting will be extended for the development of a Michelson interferometer, proper for the characterization of short light pulses spectrally localized from the UV up to the XUV, implementing special imaging techniques.

The system studied, mainly consists a Michelson type interferometer, where the beam splitter is replaced by a free standing transmission grating. Before proceed to a detailed analysis on the operation of the device, an illustration of its fundamental principles is given along with those of a Michelson interferometer.

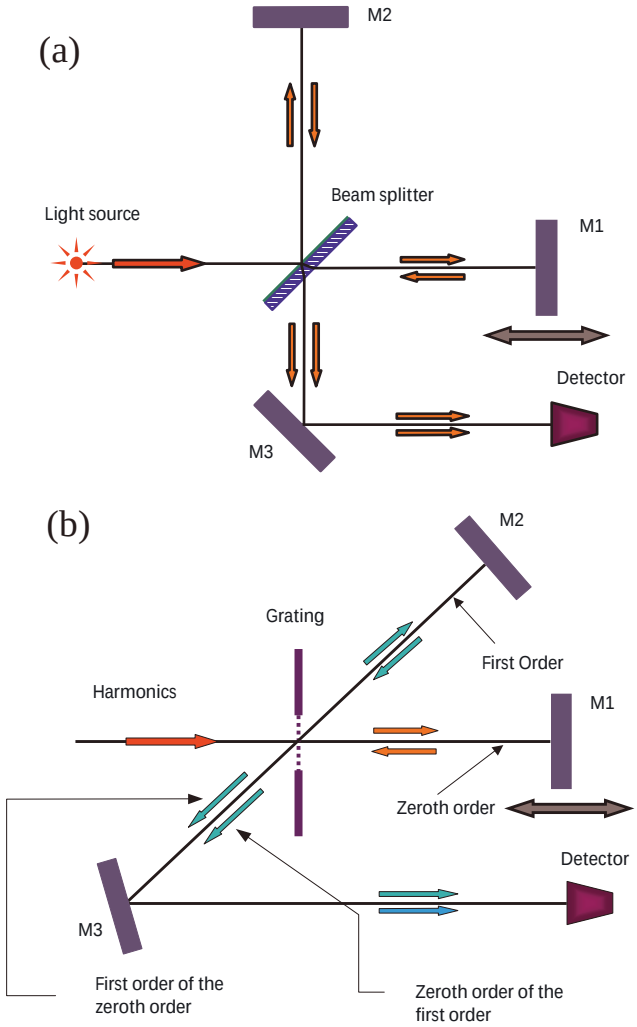

Figure 2.1: **a.** The conventional Michelson interferometer used for the characterization of femtosecond pulses. **b.** An extension of the Michelson interferometer for operation in XUV. The beam-splitter is replaced by a free standing transmission grating. M3 is dispensable for the Michelson interferometer, but it has a special contribution in the overall dispersion compensation for the grating interferometer.

In a similar manner with a conventional Michelson interferometer, light from a source is split by a transmission grating (replacing the conventional beam splitter) in its diffraction orders as illustrated in Fig2.1. A pair of mirrors M1, M2, reflect the first

and zeroth order of the refracted beam, straight back to the grating. After the second passage through the grating, the first order of the zeroth order, and the zeroth order of the first order, co-propagate and reach the screen reflected by the Mirror M3. Despite that Mirror M3 is dispensable for the Michelson interferometer, it plays an important role in the overall dispersion compensation for the grating interferometer and will be discussed in detail later. Since the number of first and zeroth order diffractions is equal for both paths described, the two arms of the interferometer possess exactly the same energy, independently of the transmission grating efficiency. Finally, for introducing the necessary delay between the two interferometer arms, Mirror M2 can be mounted to a translation unit.

2.2 Free standing transmission gratings

Due to the high absorption of materials in the XUV spectral range, high harmonics cannot propagate in general through solid or liquid matter. Propagation in gasses is possible, but even there, the pressure should be kept sufficiently low for an efficient transmission. Usually, transmission gratings are constructed by holographic ruling techniques on thin transparent material, and thus their applicability is limited at the visible or at the UV spectral region. The critical point for passing to the XUV grating beam splitting, is the so called free standing transmission gratings. In the interferometer proposed here, a free standing transmission grating is utilized, therefore a short introduction to it's characteristics is of particular interest.

A free standing transmission grating, mainly consists of a set of equidistantly arranged parallel bars, usually made of gold. Such a grating, is characterized by two main parameters; the grating constant d connected with the structure periodicity and the parameter a which is the gap between the bars. Both parameters are illustrated in Fig.2.2.a. In Fig.2.2.b a scanning electron microscopy image of a free standing transmission grating, is depicted. Commercially available gratings, have a ruling of

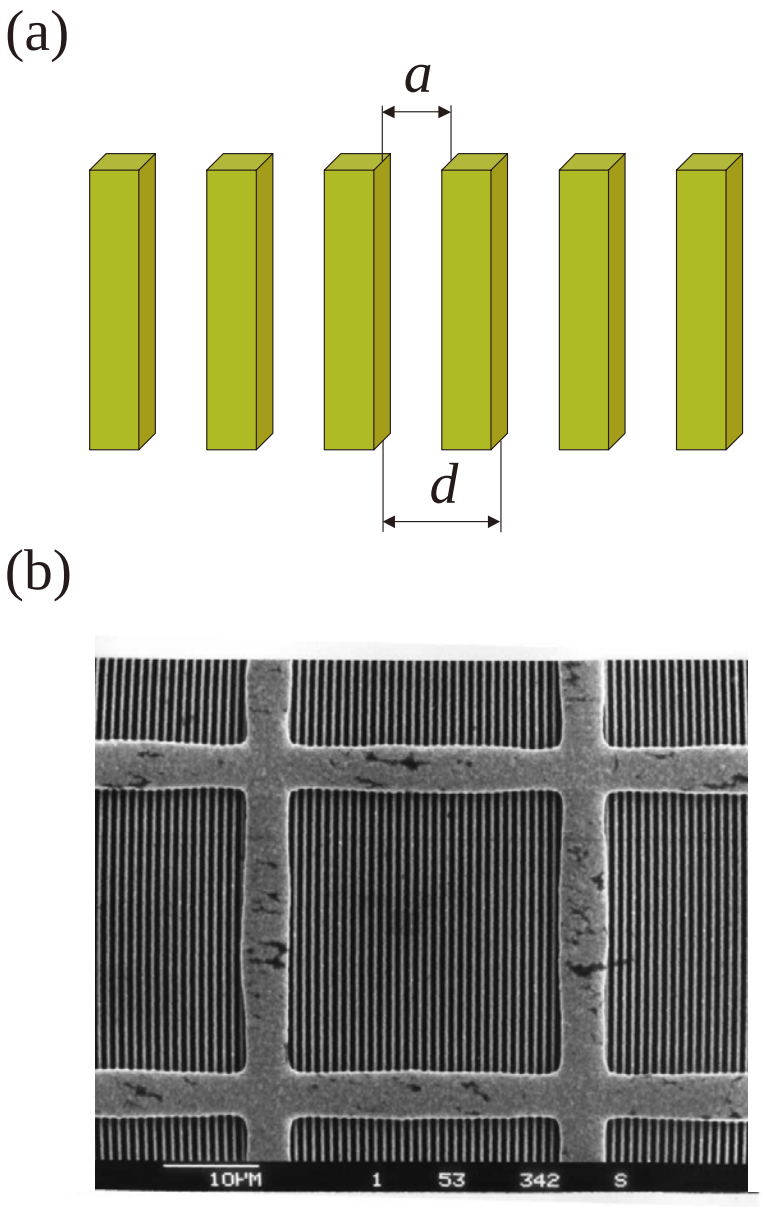

Figure 2.2: **a.** A schematic draw of a free standing transmission grating. The periodicity d and the between bars distance a are indicated. **b.** Scanning electron microscopy picture of a $1000 - \ell/mm$ grating, manufactured by Heidenhain GmbH.

$1000 \sim 2000\ell/mm$ corresponding to a constant of $0.2 \sim 1\mu m$. Due to their fragility, the gold bars are supported by a grid with typical dimensions $\sim 30d$, in order to prevent diffraction losses in the spectral range of utilization. According to Kirchhoff's theory, the efficiency of the mth-order of diffraction is given by:

$$\eta_m = \left(\frac{a}{b}\right)^2 \left[\frac{\sin(m\pi\frac{a}{d})}{m\pi\frac{a}{d}}\right]^2, \quad m = 0, 1, 2, .. \tag{2.1}$$

where m is the mth order of diffraction.

An interesting feature of the free standing transmission grating, indicated by equation (2.1), is its flat spectral response, since the efficiency is determined by the ratio a/b. For example, assuming a ratio a/b=0.5, equation (2.1) has a local maximum corresponding to the maximum intensity that a transmission grating can deliver to the first order of diffraction $\eta_1 = 1/\pi^2 \simeq 10\%$, while in the zeroth order $\eta_0 = 25\%$ of the total intensity, is delivered.

However, the flat spectral response of a free standing transmission grating, is limited within an ultra-broad band of the radiation spectrum. In the short wavelength limit approaching the X-rays, the gold bars become partially transparent to the incident radiation. This limit for a 1000 l/mm gold bar grating is at about 10 nm (Brauninger et. al.; 1979, Eidmann et. al.;1990). The long wavelength limit, is for $\lambda \sim a$ where the grating efficiency becomes strongly wavelength depended, due to resonance diffraction by the grid (Lochbihner et. al.; 1993). For the gratings proposed here this limit is at approximately 100 nm.

2.3 Dispersion compensation, using imaging configurations

A fundamental property of a transmission grating, is the introduction of angular dispersion to the diffracted radiation. On one hand, this feature of the transmission grating, allows spectral selection by utilizing geometrical apertures and obstacles,

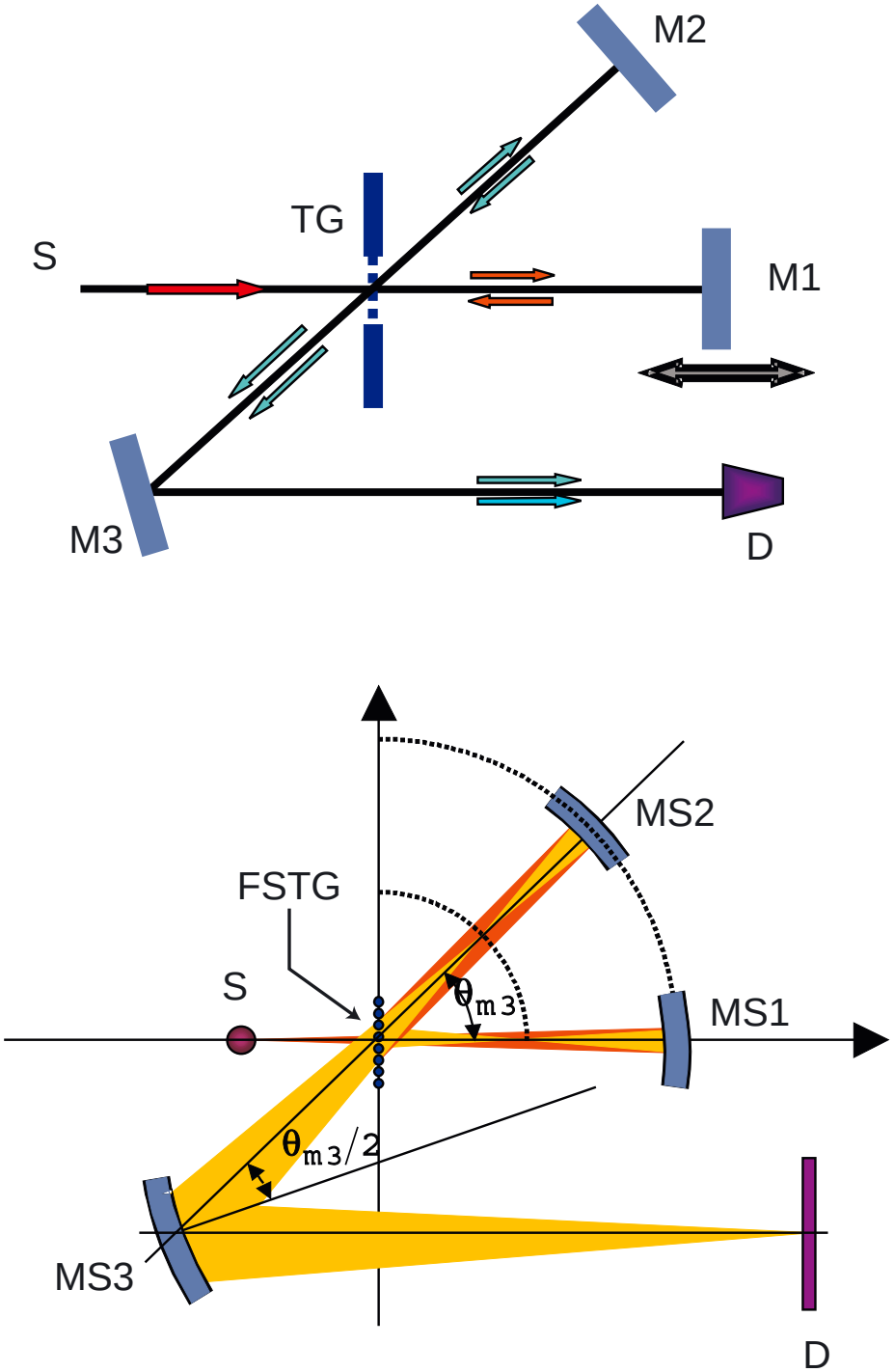

Figure 2.3: The transition to the dispersionless geometry, for the grating interferometer. MS1,MS2,MS3: Spherical mirrors, FSTG: Free standing transmission grating.

so that the desired harmonic spectrum can be selected i.e. a group of harmonics or a particular harmonic. On the other hand, in order the overall dispersion introduced by the grating to be compensated, allowing the characterization of short XUV pulses, a special design for the interferometer is required. From a geometrical optics point of view, that requires, that the total optical paths travelled by each particular spectral component of the initial pulse propagating through the interferometer, should be equal. This fundamental condition can be satisfied, if the two mirrors M1 and M2 are replaced by spherical ones, and their curvature center, coincides with the geometrical center of the grating. This transition is depicted in Fig.2.3. According to the theory of optical imaging, if this condition is preserved, each spherical mirror MS1 and MS2 images the grating surface relayed to itself. On light of that idea, since the dispersion of the beam just passed the grating surface is zero, the image also exhibits zero dispersion and therefore, the total dispersion introduced by the grating, is eliminated. A geometrical demonstration of the grating imaging, is depicted in Fig.2.4, where only chief rays are considered for schematic clarity. M3 mirror, is replaced with a spherical one (MS3). Thus MS3 together with redirecting is also focusing the output light to a screen.

2.4 Ray tracing analysis

As mentioned so far, the imaging of the transmission grating in to itself, eliminates the dispersion introduced, therefore the system is expected to be dispersionless. However, spherical abberations introduced by the mirrors, may affect the temporal profile of the examined pulse. In order to study how far these effects prevent the perfect "spatiotemporal imaging", detailed study based on ray tracing is carried out.

Ray tracing codes, have been extensively employed for the characterization of optical systems, specially when direct geometrical solutions are complicated, or even impossible. In principle, the main purpose of a ray tracing simulation is to calculate

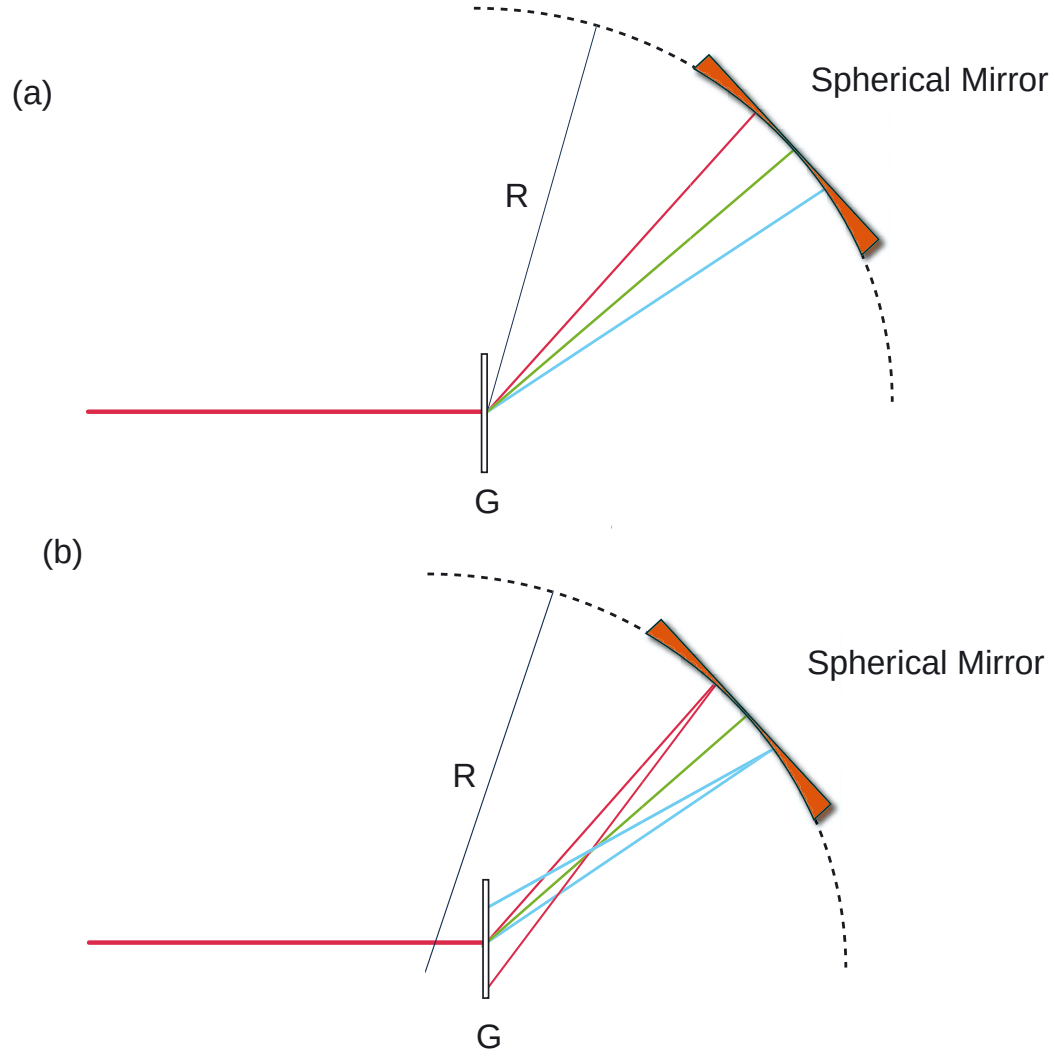

Figure 2.4: **a.** Imaging condition. The Center of the mirror is located at the geometrical center of the grating. Chief rays corresponding to different wavelength are reflected straight back travelling equal optical paths. **b.** Out of imaging condition. The optical paths travelled by the rays are unequal and intersect the grating surface to a different point.

the optical paths for a desired group of rays, used to simulate the light, travelling through the investigated optical system. In order to simulate the broad spectrum of a pulse, the discrete rays used for the harmonic beam representation, are defined to have wavelengths covering the desired spectrum. Since the optical path for every particular spectral component $\ell(\omega)$ is calculated, the parameters associated with the pulse characteristics, can be determined. It has been shown by Treacy (Treacy, 1969) that for such systems, the first derivative of the phase with respect to the frequency, the so called group delay D_1, is given by:

$$D_1 = \frac{d\phi(\omega)}{d\omega} = \frac{\ell(\omega)}{c} \tag{2.2}$$

The group delay dispersion D_2 that describes the temporal broadening is given by:

$$D_2 = \frac{d^2\phi(\omega)}{d\omega^2} = \frac{1}{c}\frac{d\ell(\omega)}{d\omega} \tag{2.3}$$

The setup is investigated in three variant geometries, referred as Case I, Case II, Case III configurations. For the Case I and Case II, we will present the calculations performed by Dr. George Tsakiris (Max Planck Institute für Quantenoptik) using a homemade two dimensional ray tracing code developed by him and it is based on the I.D.L. graphics software. The results for Case I and Case II have been also verified by a program developed on the OPTICA package of the Mathematica, proper for 3D calculations, by the author. It was found, that these cases posses an almost two dimensional character, and thus no 3D calculations were required for accessing their fundamental characteristics. Further, for the study of the 3D pulse fronts, as well as for the focusing capabilities and the effects of the abberations which are important for the estimation of the experimental feasibility of an optical arrangement, in all the cases presented here, the code developed in the OPTICA package was employed. The Case III was totally analyzed by the same code since it comprises a full 3D

arrangement.

Every particular configuration studied, posses special features and can be utilized for different purposes for accessing the temporal characteristics of harmonics. A generalized draw of the setup proposed here and analyzed by the ray - tracing codes, is depicted in Fig.2.5. A point source located at distance x_s, provides a certain number of rays. The source rays reaching the grating, placed at the center of the coordinate system, are diffracted according to the fundamental grating equation:

$$\sin\theta_{in} - \sin\theta_{out} = mN_g\lambda \tag{2.4}$$

MS1 and MS2 properly positioned, reflect the rays of the first order and the zeroth

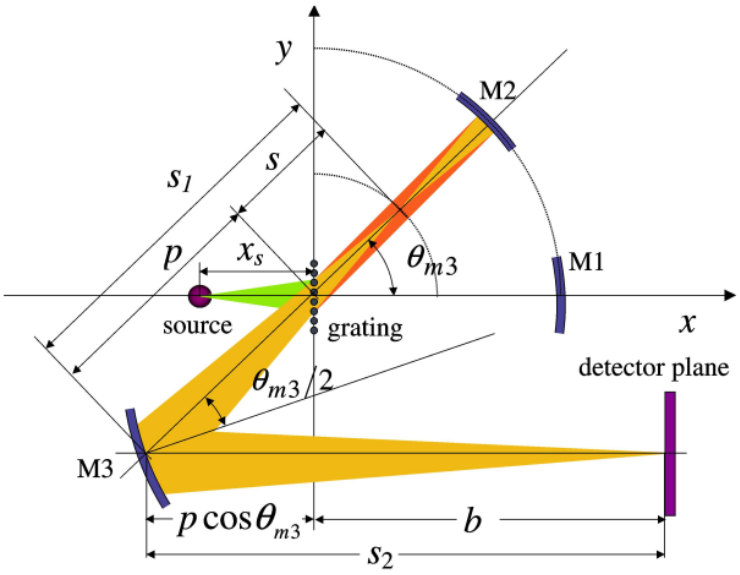

Figure 2.5: The grating interferometer global geometrical arrangement, comprises the base for all configurations studied in this work. Only the first order - zeroth order arm is depicted for simplicity. The calculation parameters used, are indicated and their values are given in the corresponding table, for every particular configuration studied.

order diffraction straight back respectively,and after the second passage from the grating, they are redirected to a screen by a third mirror MS3. The total optical path $\ell(\omega)$ travelled by every ray of a specified frequency ω, is calculated in the detector plane (screen) located at distance d from the grating. The calculation is repeated for both the arms of the interferometer i.e. the zero-first order arm and the first-zero order arm, for all the spatially distributed rays and for every frequency considered. Each Mirror used, is defined by the coordinates of its sphere center $x_{M1,2,3}$, $y_{M1,2,3}$, as well as with its curvature radius $r_{M1,2,3}$.

In all configurations studied here, MS1 and MS2 have fixed positions in order to image the grating surface relayed to itself. The position of the third Mirror MS3, is case sensitive, in order to satisfy special imaging requirements, that will be extensively analyzed in the following sections. Assuming that the chief ray of a specified harmonic is first order diffracted at an angle θ_{M3}, the angle of the MS3 in order this ray to intersect the screen perpendicular, is $\theta_{M3}/2$. This condition, simply results from a geometrical consideration of the above setup, and provides evaluation simplicity since grating and detector remain in parallel planes. Although the MS3 angle is $\theta_{M3}/2$ independently of the particular configuration, its location on the propagation axis is specified, in order to image a certain point of this axis to the detector plane. If f is the off axis focal length of MS3, $s_1 = p + s$ the distance between the object and the mirror, and $s_2 = pcos\theta_{M3} + b$, the distance between the image and the mirror, then the above variables are related as:

$$\frac{1}{p+s} + \frac{1}{pcos\theta_{M3} + b} = \frac{1}{f} \tag{2.5}$$

Due to the associated astigmatism, spherical mirrors posses two focal lengths when the are used in off-axis geometries. These two focal lengths correspond to the so called tangential focus $f_t = r\cos(\theta_{M3}/2)/2$, located in the plane of incidence and the sagittal $f_s = r/\cos(\theta_{M3}/2)/2$ focus, lying in a perpendicular plane. In the arrangement studied here, MS3 mirror is in an off-axis configuration, therefore a spatial separation of foci is taken in to account.

2.4.1 Case I

Since MS1 and MS2 are properly positioned providing an 1:1 imaging of the grating relayed to itself, the third mirror MS3 in a similar manner, images the grating to the screen (detector plane). In other words, the zero dispersion grating surface image, is transferred through the optical system to the screen.

λ_L	(μm)	0.8	r_{m1}	(cm)	30
N_g	(ℓ/mm)	1000	x_{m1}	(cm)	0
s_g	(μm)	350	y_{m1}	(cm)	0
x_s	(cm)	-20	r_{m2}	(cm)	30
n_1		25	x_{m2}	(cm)	0
n_2		37	y_{m2}	(cm)	0
n_{hc}		31	r_{m3}	(cm)	60
s	(cm)	0	x_{m3}	(cm)	13.9
s_1	(cm)	46	y_{m3}	(cm)	-0.41
s_2	(cm)	86	b	(cm)	40
D_2	(fs^2)	$< 1.0^{-3}$			

Table 2.1: Parameters used for the ray tracing of the Case I.

For the ray tracing analysis, we consider a source, emitting odd harmonics of the fundamental of a Ti:Saph laser at $\lambda_L = 0.8\mu m$ from $n_1 = 25$ to $n_2 = 37$. As central harmonic, the $n_{ch} = 31$ is defined. The ray tracing code, calculates the optical paths for the chief ray of every harmonic, as well as for its marginal rays travelling the path between the source and the detector plane. The parameters used in the calculation are listed in Table 2.4.1, while the results are depicted in Fig.2.6. The setup is depicted in Fig.2.6.a. and the optical paths are shown. The pulse front tilting for all harmonics and both arms as a function of spot radius r_s defined in the grating, is plotted in Fig2.6.b, yielding to a pulse front tilt. The difference in arrival times between the chief ray of every particular harmonic of the desired spectrum, and its extreme paraxial, $\Delta l^{(n)}_{front} = l^{(n)}_{paraxial} - l^{(n)}_{chief}$ for both the arms of the interferometer at the detector plane is calculated and it is depicted in Fig.2.6.d, indicating that the

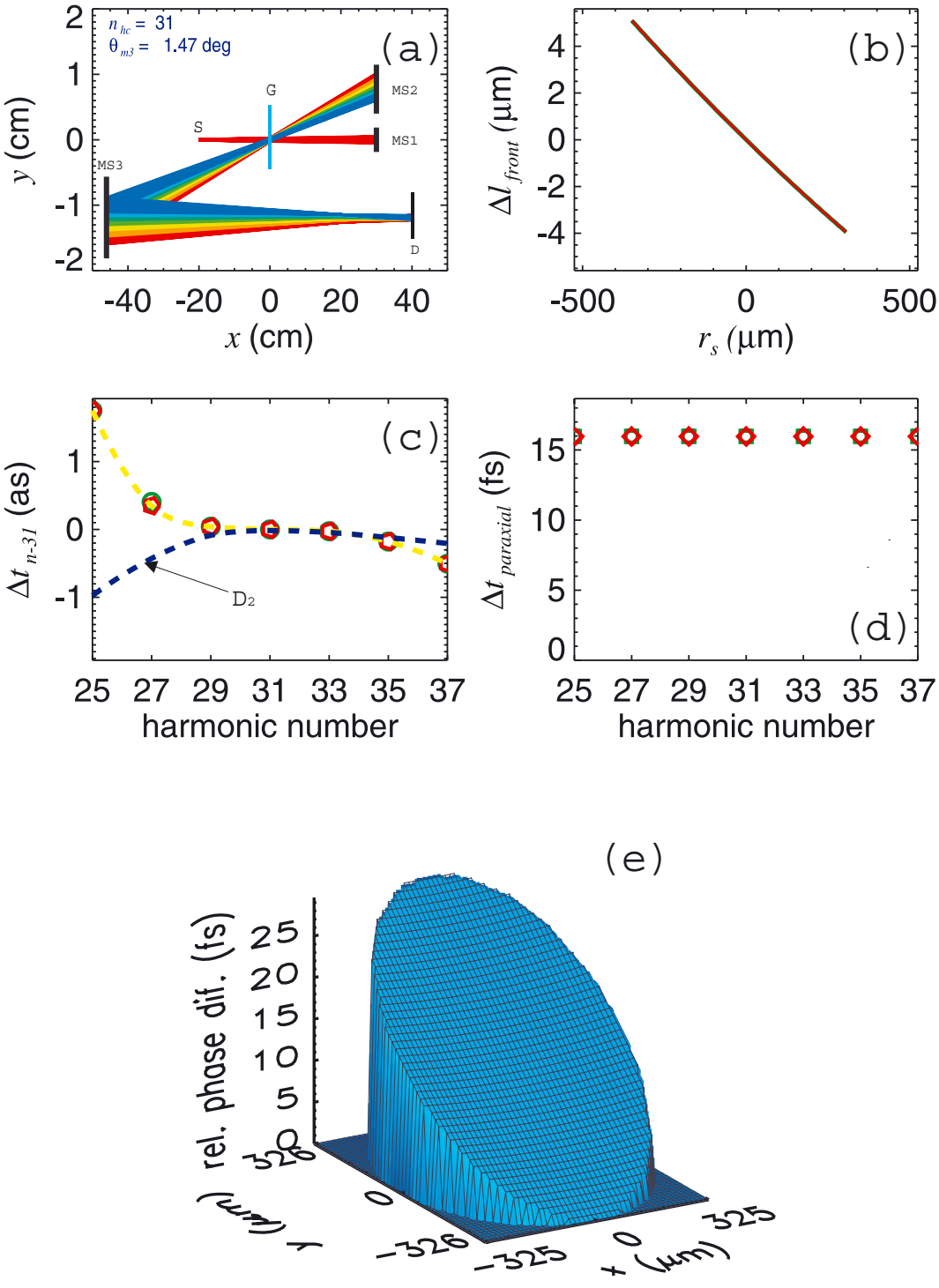

Figure 2.6: Ray tracing results case I. The grating is imaged to the detector plane (s=0). **a.** Optical paths for the harmonics between $n_1 = 35$ and $n_2 = 37$, for both the arms of the interferometer. **b.** Pulse front tilting as a function of spot radius r_s for all harmonics and both arms. **c.** The group delay relative to the $31th$ harmonic yellow line. Dark dashed line: The group delay dispersion. **d.** The difference in arrival times between the chief ray of every harmonic and its extreme paraxial for n=25-37 harmonics. The symbol denotes the two arms of the interferometer (red squares zero-first, yellow squares first-zero). **e.** A 3D plot of the pulse front at the detector plane as it is reconstructed introducing a sufficient number of rays in the simulations performed using the OPTICA.

tilt angle is the same for all the harmonics. Further, the key result of this simulation is the extremely low dispersion introduced to the propagating beam. In Fig.2.6.c, a direct comparison between chief rays optical paths and for all the selected harmonics is depicted, as a difference in their arrival time on the screen related to the 31th harmonic representing the group delay. The resulting group delay dispersion is obtained by the differentiation of the smooth spline interpolation of the group delay, and it is approximately $D_2 = 1\ as^2$. According to the equation (1.8), it is acceptable even for the characterization of pulses having duration of a few tens of attoseconds. Additional results related with the pulse front at the detector plane, in a 3-D more detailed approximation is presented in Fig.2.6.e. The pulse profile presented, is reconstructed by considering a reasonable number of rays, covering the input beam spatial profile. The rays included, are associated only with the $31th$ harmonic for clarity. Finally, the spot size at the detector plane, is calculated to be $\sim 650\mu m$. This size is connected mainly with input aperture of the system, and the divergence of the harmonics produced in the laser focus.

2.4.2 Case II

In this configuration, instead of the grating, the harmonics source is imaged relayed to the screen. Assuming again a point source of harmonics at distance x_s (see Fig.2.5), MS1 and MS2 mirrors image this source in the space behind the grating, forming a virtual source. Further, according to equation (2.5) the third's mirror MS3 position, is determined in order to image this virtual source to the screen. This condition is satisfied because of the spherical abberations introduced by the mirrors MS1 and MS2, the image of the source, is split into several point images. This spatial splitting of foci behind the grating, is therefore imaged to the screen by the MS3 as well.

The component parameters used in the ray-tracing for this configuration are listed in Table 2.4.2. As depicted in Fig.2.7.a foci are spatially separated at the screen and

λ_L	(μm)	0.8	r_{m1}	(cm)	30
N_g	(ℓ/mm)	1000	x_{m1}	(cm)	0
s_g	(μm)	350	y_{m1}	(cm)	0
x_s	(cm)	-20	r_{m2}	(cm)	30
n_1		25	x_{m2}	(cm)	0
n_2		37	y_{m2}	(cm)	0
n_{hc}		31	r_{m3}	(cm)	60
s	(cm)	8.57	x_{m3}	(cm)	20.4
s_1	(cm)	48.1	y_{m3}	(cm)	-0.25
s_2	(cm)	79.5	b	(cm)	40
D_2	(fs^2)	< 1.0			

Table 2.2: Parameters used for the ray tracing of the Case II.

dispersion arises affecting the output pulse duration. Further, in Fig.2.7.b a slight difference in tilt between fronts corresponding to the two arms is present, as well as for different harmonic orders in Fig.2.7.d connected with the spherical abberations introduced. The focus size is calculated 0.35 μm, indicating the possibility of utilization of this configuration for high intensity output requirements. A 3-D representation of the pulse front in the focus for the 31th harmonic, is shown in Fig.2.7.e. The substructures on the pulse front surface, are due to numerical uncertainties. For the spectral range which is kept the same as in case I, the group delay dispersion that harmonics undergo on the screen is of the order of 1 fs^2, see Fig.2.7.c. As expected, since the grating surface is not imaged-relayed to the screen, the setup is not dispersion free. However the calculated value for the dispersion, is still quite low and acceptable for the characterization of single harmonic pulses, which are expected to posses duration of a few tens of femtoseconds. In Chapter 3 of this thesis, an experimental implementation of case II configuration for the temporal characterization of the third harmonic of a Ti:Sa laser, will be presented.

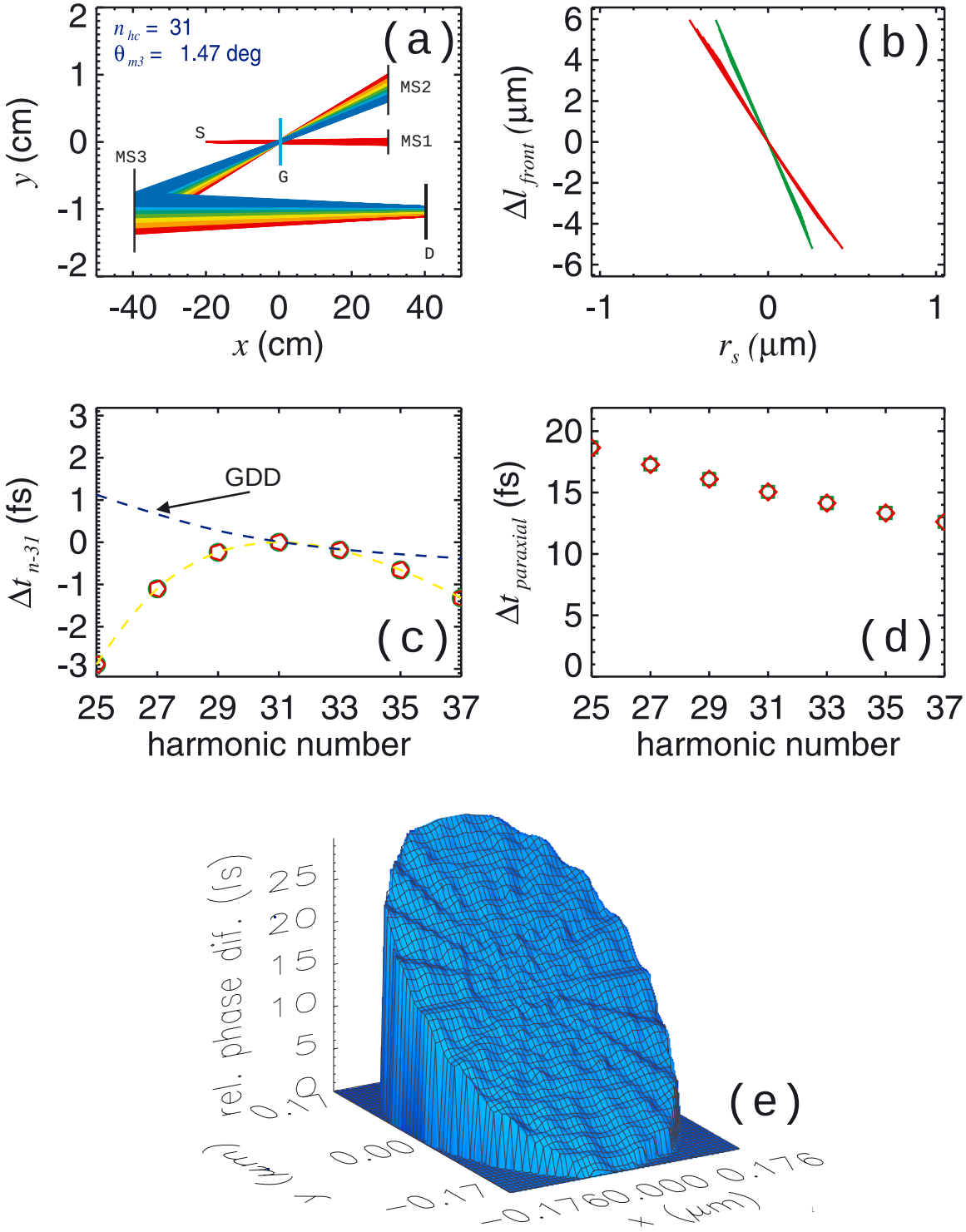

Figure 2.7: Ray tracing results case II. The source is imaged-relayed to the detector plane (s = 8.57 cm). **a.** Optical paths for the harmonics between $n_1 = 35$ and $n_2 = 37$, for both arms of the interferometer. **b.** Pulse front tilting as a function of spot radius r_s for all harmonics and both arms. **c.** The group delay relative to the $31th$ harmonic yellow line. Dark dashed line: The group delay dispersion. **d.** The difference in arrival times between the chief ray of every harmonic and its extreme paraxial for n=25-37 harmonics. The symbol denotes the two arms of the interferometer (red squares zero-first, yellow squares, first-zero). **e.** A 3D plot of the pulse front at the detector plane as it is reconstructed, introducing a sufficient number of rays in the simulations performed using the OPTICA.

2.4.3 Case III

In what follows, a novel configuration possessing a full combination of the advantages of the two previous arrangements, is presented and analyzed. Following Fig.2.8 harmonics produced in NLM-1 co-propagate with the fundamental and impinge to the transmission grating. The zeroth order of diffraction is reflected straight back by the MS1, while the one of the first orders which is spectrally analyzed, is reflected by the mirror MS2. MS2 in a similar manner with the cases studied till now, is properly positioned in order to image the grating relayed to itself. Both mirrors MS1 and MS2, are slightly tilted in such a way, that the back reflected harmonic beams are somewhat elevated, related to the incoming ones.

Finally, a third mirror redirects and focuses the first order of the second diffraction together with the fundamental, to a second nonlinear medium. In Fig. 2.8 a top and a side view of the setup described is depicted, while a 3-D representation of the setup is depicted in Fig. 2.8.b. The setup characteristics, have been analyzed in a similar manner with the previous two cases. The NLM-1, is simulated by a point source, and a screen is placed in the position of the NLM-2, where the characteristics of the outgoing focused beam are studied. In addition, a new parameter h indicating the back-reflected harmonic and fundamental beam elevation measured on the grating, is introduced. The parameters used for the simulation, are listed in Table2.4.3. The setup is examined for three values of the elevation h, and the results are summarized in Fig.2.9 where the pulse front tilt Fig.2.9.a, the group delay Fig.2.9.b and the group delay dispersion Fig.2.9.c are shown.

The pulse front tilting that arises, is lower than 10 as and becomes less when the harmonic order increases. The group delay dispersion introduced to the harmonics, is even for an elevation value of $h = 5mm$ less than a 1.5 as^2, indicating that the interferometer could be employed for the characterization of attosecond pulses. A 3-D representation of the pulse front as it is reconstructed by a large number of rays at the

λ_L	(μm)	0.8	r_{m1}	(cm)	30
N_g	(ℓ/mm)	1000	x_{m1}	(cm)	0
s_g	(μm)	350	y_{m1}	(cm)	0
x_s	(cm)	-20	r_{m2}	(cm)	30
n_1		25	x_{m2}	(cm)	0
n_2		39	y_{m2}	(cm)	0
n_{hc}		31	r_{m3}	(cm)	60
s	(cm)	8.57	x_{m3}	(cm)	20
s_1	(cm)	48.57	y_{m3}	(cm)	0.1
s_2	(cm)	78.45	b	(cm)	38.45
D_2	(fs^2)	$< 1.210^{-3}$			

Table 2.3: Parameters used for the ray tracing of the Case III.

focus, is shown in Fig.2.9.d. The additional substructures shown, are associated with the abberations introduced by the mirrors but since they correspond to some tenths of an attosecond the distortion introduced to the pulse front in the focus region, is negligible. The diffraction free focus size, is calculated to be of the order of some tenths of a micron, indicating that the arrangement could supply with tide focused harmonics in its output.

2.5 Efficiency estimates and outlook

In this section, estimations on the efficiency and the experimental feasibility of the configurations proposed in this chapter, will be presented. The setup proposed in Case I, can be employed for single order field autocorrelation, of a single or a group of harmonics. The high spectral selectivity achieved by mechanical obstacles and its flat spectral response due to the free standing transmission grating utilization, allows the reveal of the spectral information, as well as of the temporal coherent length of the studied harmonic radiation.

The temporal characterization of a single harmonic, can be performed using the arrangement of the Case II. In order for this setup to be appropriate for determining

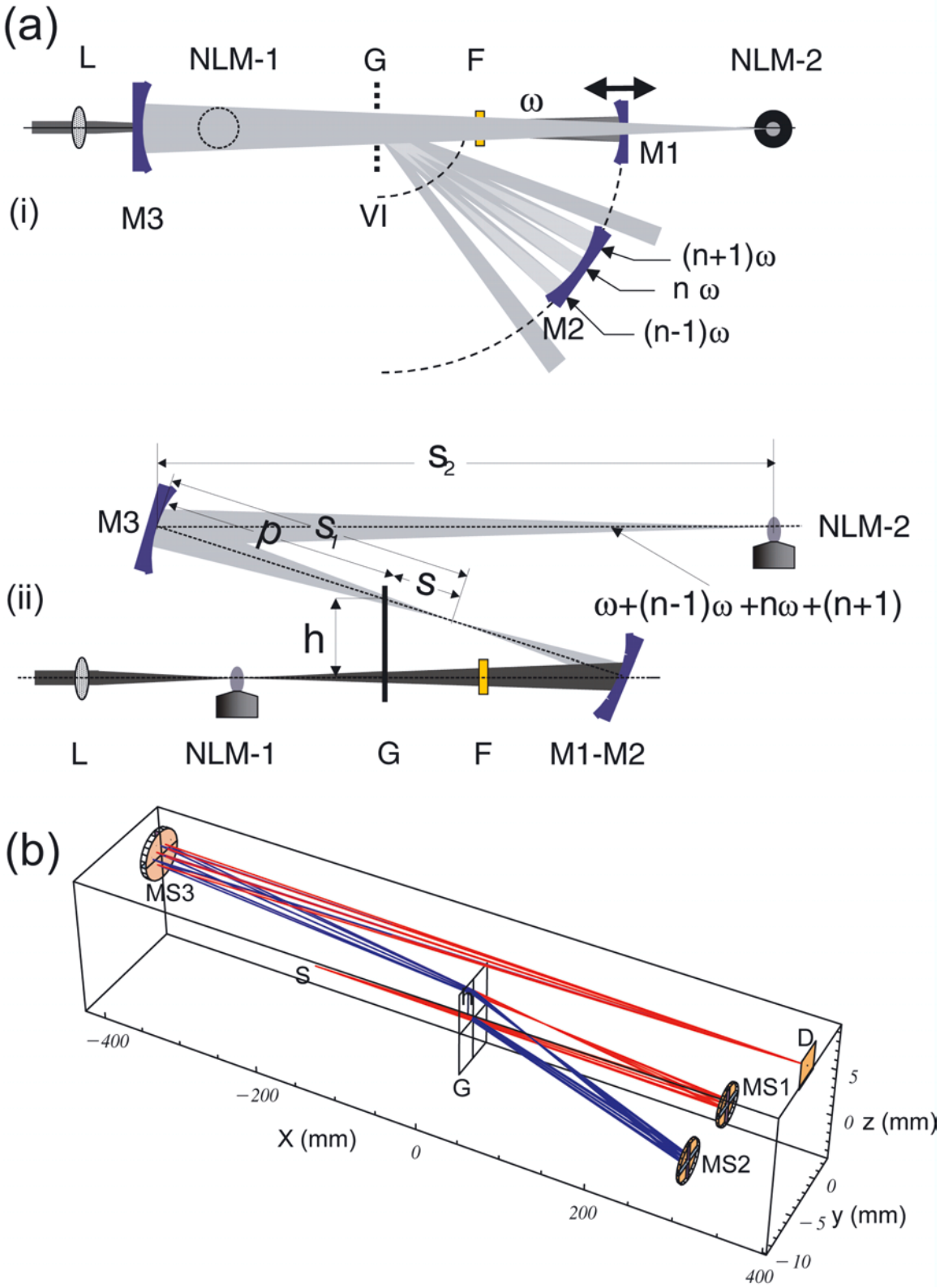

Figure 2.8: The case III optical arrangement. **a.(i)** Top view, **a.(ii)** Side view. **b.** Full 3D view constructed by the OPTICA code.

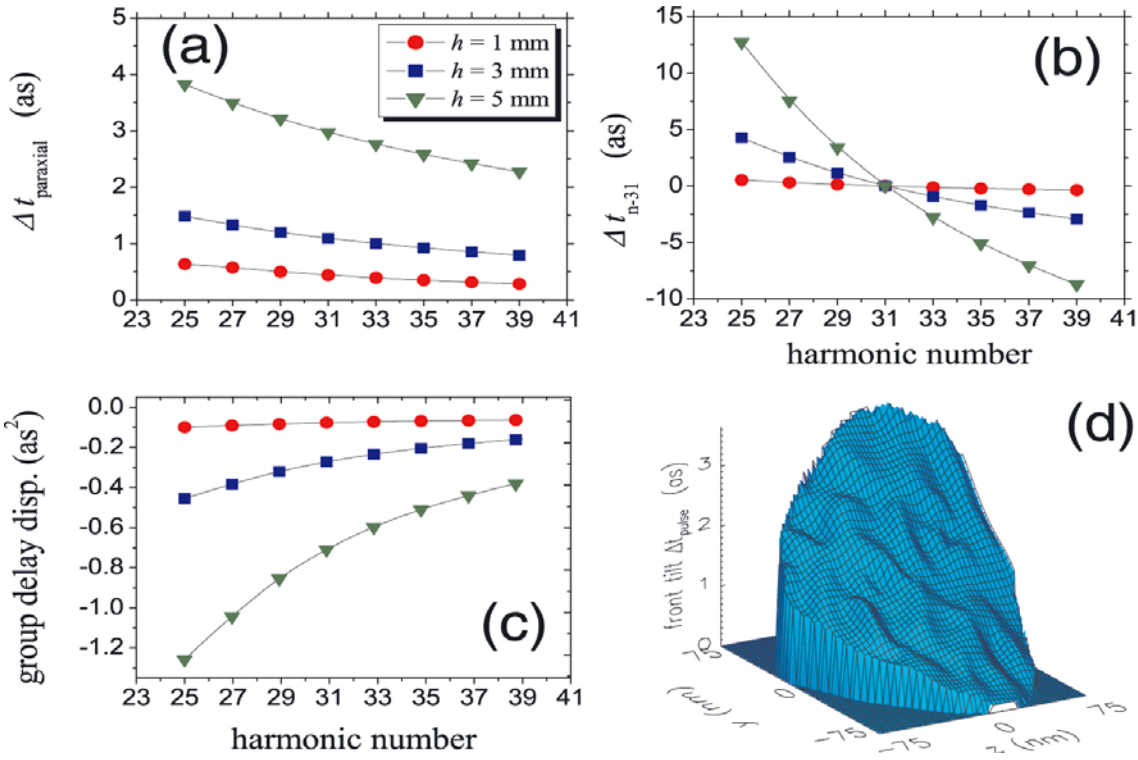

Figure 2.9: Ray-tracing results for case III with the indicated value for the elevation h and for the harmonics n=25-39. **a.**The difference in arrival times between the chief rays and the extreme paraxial ray. **b.** The group delay. **c.**The group delay dispersion obtained by differentiation of the smooth spline-interpolation of the group delay. **d.** A 3D plot of the harmonic beam spot on the detector plane.

the duration of a harmonic, two conditions must be fulfilled. The first one, is the low dispersion that the system must introduce to the studied harmonic. This can be achieved, if the harmonic to be characterized, is taken as the central harmonic in the implementation of the interferometer. A local minimum in the group delay associated with the central harmonic (see Fig.2.7), together with the relative narrow bandwidth of the harmonic (compared with that of the studied region in Fig.2.7), provides the low dispersion necessary for that application. The second condition is connected with the intensity in the focus, which is directly associated with the overall efficiency of the interferometer. In our estimations, we will assume the utilization of a free standing transmission grating, similar with that described in the relevant section of this chapter e.g. $1000\,l/mm$ and $a/b = 0.5$. The total efficiency of a sequential first order - zeroth order passing is $0.1 \times 0.25 = 0.025$. Assuming that gold mirrors are utilized with reflectivity $R_G = 10\%$ at the 50-100 nm spectral regime, an overall system efficiency of $\simeq 2.5\,10^{-4}$ is resulting. Second order autocorrelation of the 9^{th} has been reported (Kobayashi *et al.*; 1998) where the two photon ionization of He, has been utilized as a nonlinear process. In this experiment, the harmonic intensity was estimated to be $I_9 \simeq 0.15\,10^{12}\ W/cm^2$. Assuming that this intensity would be sufficient for registering a second order autocorrelation, and taking in to account the overall efficiency and the focus dimension calculated for the Case II, a $10^{-6} - 10^{-7}$ conversion efficiency in the harmonic generation volume would be required. This efficiency, which is trivially realizable has been exceeded with modern harmonic generation techniques (Hergott *et al.*; 2002), utilizing long focal length lenses, where a conversion efficiency of 10^{-4} for the plateau harmonics is reported.

However, the cross section of short wavelength pulses interacting with matter is rapidly decreased with the wavelength, following a rule of $\sim \lambda^6$, introducing a frontier to the application of autocorrelation methods approaching the X-ray regime. A way to access that spectral regime, seems to be the cross - correlation techniques mentioned in Chapter 1. An ideal setup for the experimental implementation of cross correlation

methods, is that proposed in case III. It combines dispersionless operation together with tight focusing of harmonics and fundamental, and allows to accurate introduce delay between fundamental and harmonics since the MS1 mirror can be mounted in a stepper translator. Back in Fig.2.8, in order to eliminate harmonics from the zero-zero order branch, a filter can be introduced. Further, a few estimations connected with the experimental feasibility of the case III configuration will be illustrated. Assume a seven photon ionization process, involving the fundamental and a single photon contribution by its seventh harmonic. For the fundamental no estimates are necessary, since the intensity is high enough after the overall loses, in order even to saturate the process. For the seventh harmonic, assuming a cross section of $\sigma \sim 10^{-18} cm^{-2}$ a focus size of $10^{-12} cm^3$ and a duration $\tau_7 \approx 10 fs$, the resulting intensity for generating a N=10 number of ions is calculated to be $I_7 = 10^3\ W/cm^2$ in the interaction volume. Assuming a 10^{-4} overall losses in the grating interferometer, a harmonic intensity of $10^7 W/cm^2$ would be necessary in the generation. This would require a conversion efficiency of about 10^{-7}, which is according to the previous discussion experimentally feasible.

Chapter 3

Application of the grating interferometer, for the temporal characterization of the third harmonic of a Ti:Saph laser, produced in Argon gas

3.1 Introduction

In the previous chapter, we presented and analyzed in detail the fundamental properties of a grating based Michelson interferometer and we investigated the possibilities,of employing such a device, for accessing the temporal characteristics of XUV harmonics, or even attosecond pulses. Here, the utilization of the grating interferometer for the characterization of the third harmonic of a Ti:saphire laser produced in argon gas, will be demonstrated. The purpose of these experiments is twofold: To experimentally test the interferometer and to verify the results of the ray-tracing. Additionally, to perform the first experiments towards the characterization of high harmonics and harmonic superpositions using the grating interferometer. Having these aims in mind, even if third harmonic production could be more efficient and stable utilizing a four wave mixing scheme in a set of nonlinear crystals, in these experiments the evaluation of a generation scheme in a rare gas, keeps the application of the grating interferometer close to the conditions of high harmonic production, which

is efficient only in gaseous media so far. According to the previous chapter, the implementation of the grating interferometer for the temporal characterization of a single harmonic, would require the evaluation of the Case II configuration. Calculation for the third harmonic in a case II configuration resulted to a $D_2 \leq 8fs^2$, as well as to a relative pulse front tilting between the two arms of 14^o. This dispersion introduced by the interferometer is quite low and acceptable for pulses of $T_p \geq 10fs$ according to the equation (1.8). Assuming a peturbative generation of the third harmonic when 45 fs pulses are focused in a gas, its duration will be about $T_{3\omega} = 25fs$. Thus the pulse duration of the third harmonic remains practically unaffected, when the grating interferometer is utilized for its temporal characterization.

This chapter is structured as follows: Initially the apparatus used for the experiment will be described, and a detail discussion of the particular components playing a critical role in this implementation will be given. Further, the experimental tests and results concerning the third harmonic pulse measurement, will be presented.

3.2 Experimental Apparatus

The experimental apparatus, comprises an implementation of the case II described in chapter II of the present thesis. Following Fig. 3.1, laser pulses are focused by 35 cm lens in a champer, containing argon gas at 300 torr. After a short propagation in the air, which filters all the high harmonics, ω and 3ω are impinging to the grating, where the 3ω is separated by the fundamental. Following the configuration of case II, a third mirror MS3 focuses the output of the interferometer to the detector champer, containing the gaseous toluene. The electron-ion signal, resulting from the toluene ionization, is amplified using a lock-in amplifier SR810 of Stanford Research, and stored in a computer.

For introducing temporal delay between the interferometer arms, MS1 is driven by a step translator of Physik Instrummente. The translator unit was well characterized

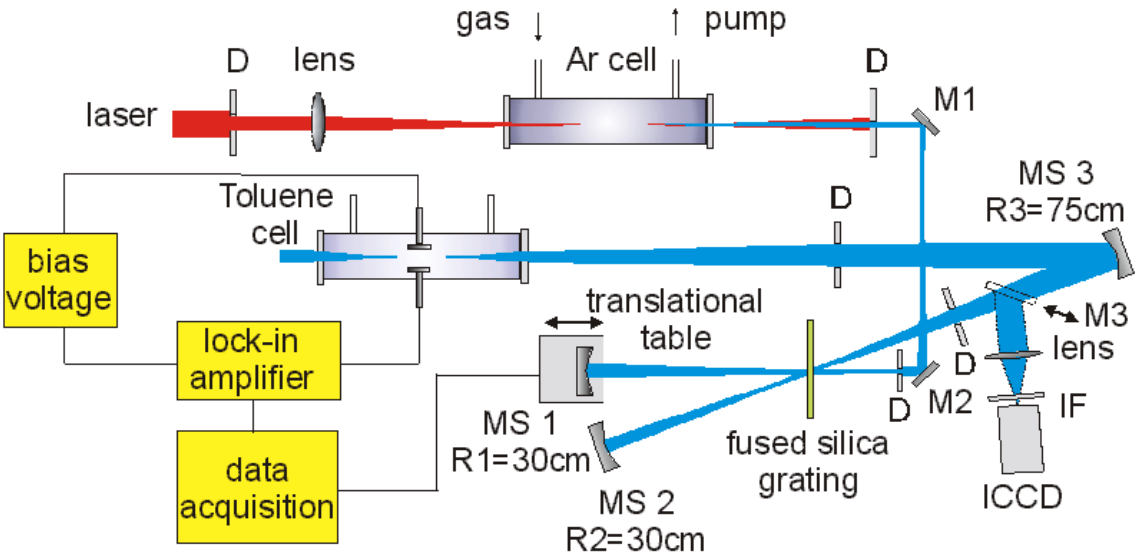

Figure 3.1: The Experimental setup. MS1,2,3: spherical Mirrors, D: diaphragm, M1,2,3: flat mirrors, IF: IR filter, ICCD: Intensified CCD camera.

in past experiments and provides a minimum step of 5 nm (measured) corresponding to delay of 15 as. For the third harmonic however, a step of 0.15 fs is sufficient for registering clear interferometric traces. The setup is additionally utilized by a ICCD camera, recording a small reflection of the beam before the MS3 supporting optical diagnostics together with the signal registration.

3.2.1 The femtosecond laser system in IESL

The ultrafast laser system employed in this experiment, comprises a commercial Coherent/B.M. Industries system, utilizing a combination of a MIRA oscillator and a kHz two stage amplification configuration.

The oscillator which is based on a Ti:Saph, Kerr lens mode locking configuration, is pumped by a 5 W, CW diode laser (VERDI COHERENT) and generates pulses of 25 fs at 800 nm, 82 MHz repetition rate, having a pulse energy of 5 nJ.

The generated pulses, are stretched up to 1000-5000 times their initial temporal duration using a grating - spherical Mirror stretching arrangement, before they seed the amplification stages, in order to prevent optical damage which may arise because

of the extremely high intensity. The first amplification stage comprises a so called regenerative amplifier, where selected pulses are trapped in, using Pockels Cell based polarization switching. The active medium of the regen is a Ti:Saph pumped by a 1064 nm crystal doubled Nd:YLF laser (532 nm) at 10 W. The amplifier outputs pulses with 1.5 mJ/pulse at 1 kHz repetition rate.

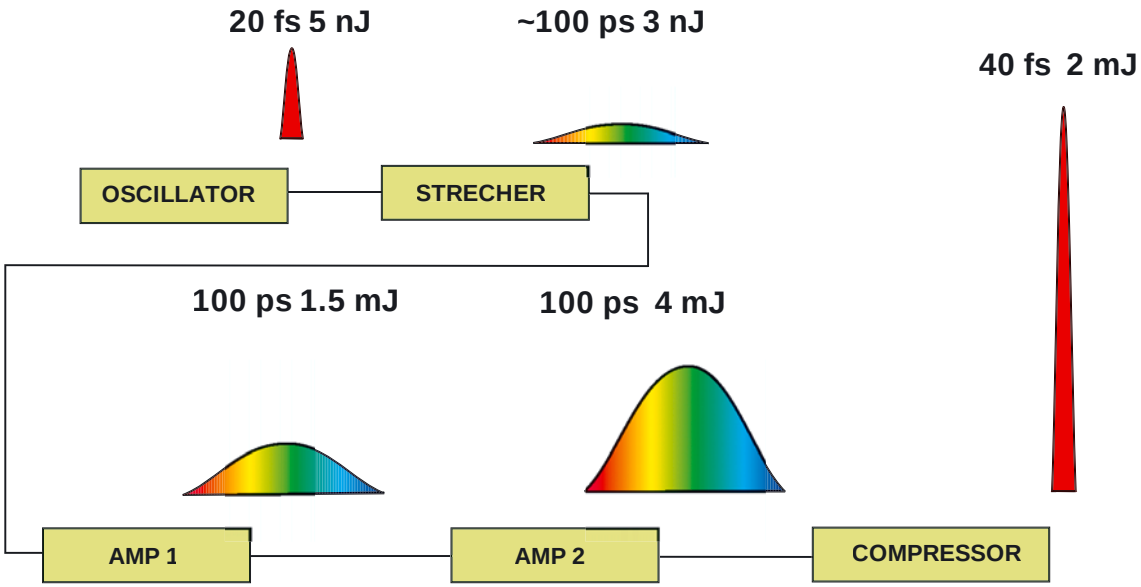

Figure 3.2: Pulse evolution, through the amplification stages. Pseudo-colors are used to indicate the pulse chirp, acquired in the stretcher.

The second amplification stage is based on a multi-pass amplifier configuration, where the pulses are amplified up to $\sim 4mJ$, again using Ti:Saph as an active medium. Finally, the pulses are compressed by a grating - pair compressor in to 40 fs duration, having energy of 2.5 mJ/pulse. This output is satisfactory for a wide variety of experiments, concerning multiphoton processes, harmonic generation, coherent control as well as material characterization e.t.c.

In Fig.3.2 the pulse evolution through the amplification stages, is depicted. The chromatic shift along the temporal profile of the pulses, indicates the chirp acquired in the stretcher unit.

3.2.2 Third harmonic generation

The laser light is focused in a static cell, containing Ar gas. The third harmonic light generated is strongly depended on the Ar pressure and this can be attributed to the phase matching effects in the generation volume. Experimentally we found that the maximum generation efficiency, is obtained when the Ar pressure in the gas static cell is stabilized at approximately 300 torr. Additionally, the beam profile of the generated third harmonic is homogeneous, providing easy alignment for the interferometer and tide focusing on its output.

3.2.3 Transmission Grating

As mentioned in Chapter II, the utilization of a free standing transmission grating, is a unique step through the dispersionless XUV interferometry. However, its flat spectral response is limited when it operates in wavelengths $\lambda \geq a$ defined in Chapter 2. For commercially available free standing transmission gratings this limit is approximately ($\sim$ 100 nm). Therefore, in order to overcome low efficiency effects, as well as spectral truncation on implementing the interferometer for measuring the pulse duration of the third harmonic, a fused silica 1 mm thick, transmission grating with $600l/mm$ was employed. This grating was specially fabricated, with its blazed angle corresponding to the third harmonic central wavelength (267nm) deflection angle. After this optimization step, the grating distributes a 20% to the first as well as to the zeroth order, providing a significant increase, to the overall system efficiency.

3.2.4 Al-coated spherical mirrors

Although gold mirrors were most appropriate for high harmonics, especially in grazing incidence geometries, due to the high reflectivity of gold, their reflectivity in the UV spectral range is quite low, reducing the efficiency of the interferometer. In order to optimize that factor for a near UV implementation of the interferometer, a set

of Al-coated spherical mirrors were utilized providing, a reflectivity higher than 90% and the highest possible energy output.

3.2.5 Detection

Detection Champer

The detection champer containing the gaseous toluene, is equipped with two electrodes for ion-electron acquisition, biased at 200V. A mechanical pump and a vacuum detector, provide a full control of the toluene gas pressure in the champer, allowing signal optimization and further studies of third harmonic pulse propagation in that medium.

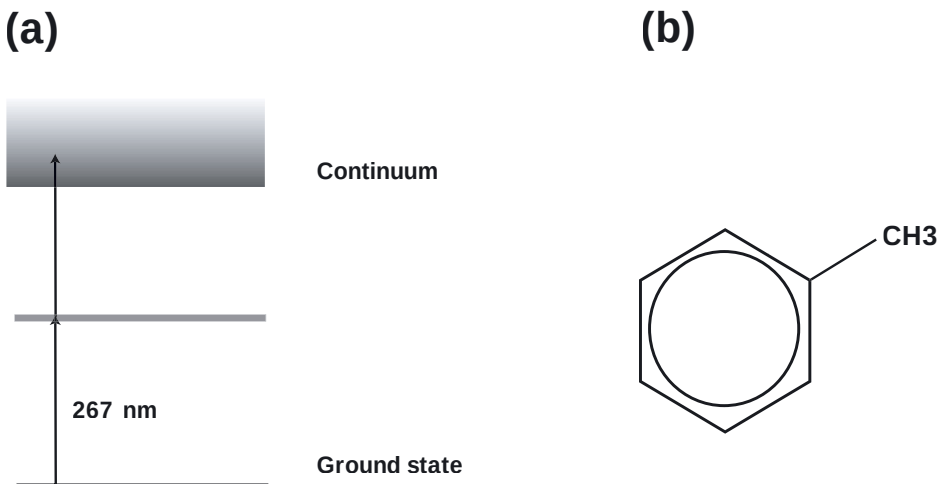

Figure 3.3: **a.** Near resonance, two photon ionization scheme for the toluene molecule. **b.** The chemical structure of the toluene molecule.

Toluene Gas

The detection of the third harmonic, and specially the nonlinear material used in order to achieve a well observed two photon signal, necessary for a temporal characterization of the third harmonic, is of particular interest and will be discussed in detail. Albeit several optical materials posses the necessary response for single order effects at the UV spectral regime, a second order well observable process even in 267 nm, is not trivially realizable. Up today, specific detectors based on SiO_2 (Streltsov *et al.*; 1998) and nonlinear absorption of Diamond (Dadap *et al.*; 1991) have been utilized for achieving nonlinear detection in the UV spectral regime. However, the intensity required in order to obtain a reliable signal, is rather high and therefore they have to be used with very low loss optical systems. In this experiment, the gaseous toluene C_7H_8 which is possessed by a wide intensity range of well observable nonlinearity, was utilized as nonlinear detector.

The ionization potential of the toluene is 8.81 eV, thus two photon ionization with the third harmonic of a Ti:Saphire laser 2x 4.65 eV is possible. The single photon absorption cross section of gaseous toluene, is depicted in Fig.3.4. The existence of a resonance absorption line of the molecule lying at 267 nm, increases the molecule ionization probability. In that case strictly speaking, the scheme of ionization is an one photon enhanced two photon ionization. The two photon ionization scheme of toluene, is depicted in Fig.3.3, where the intermediate horizontal line represents the toluene resonance.

In order to experimentally investigate the nonlinearity of the scheme proposed above, the two photon toluene ionization yield, is measured as a function of the intensity of the third harmonic produced in argon. The initial TH beam is split using a pellicle. A small fraction of the beam is recorded by a photodiode, while the rest is focused in the detector cell containing the gaseous toluene. The intensity of the third harmonic is varied by modulating the laser energy, instead of using intensity filters

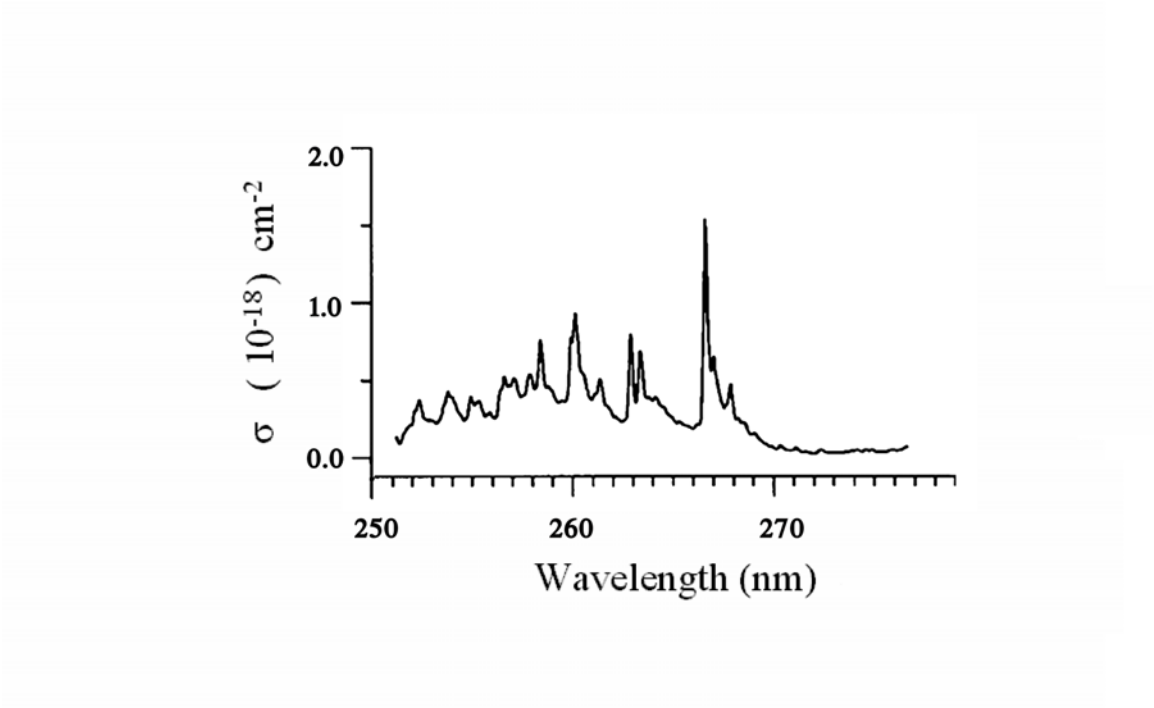

Figure 3.4: Absolute absorption cross section for the toluene molecule, in the near UV spectral region. A resonance line at 267 nm, corresponds to the transition from the ground to the first exited state of the molecule.

for the UV. This technique posses no temporal broadening, that a UV filter may introduce. Additionally, since the generation of the third harmonic can be reasonably assumed to be a perturbative process, its duration has no laser intensity dependance. A typical log-log plot of the two photon ionization yield as a function of the intensity of the third harmonic, is depicted in Fig.3.5. The intensity dependance was found to be linear with a slope of 2, typical for second order nonlinear processes.

ICCD camera

An Intensified-CCD camera, having its detection range in the near UV is employed for studying the pulses overlapping, and for the investigating of the pulse front tilting effects, by monitoring the spatial intensity fringes distribution at the interferometer output.

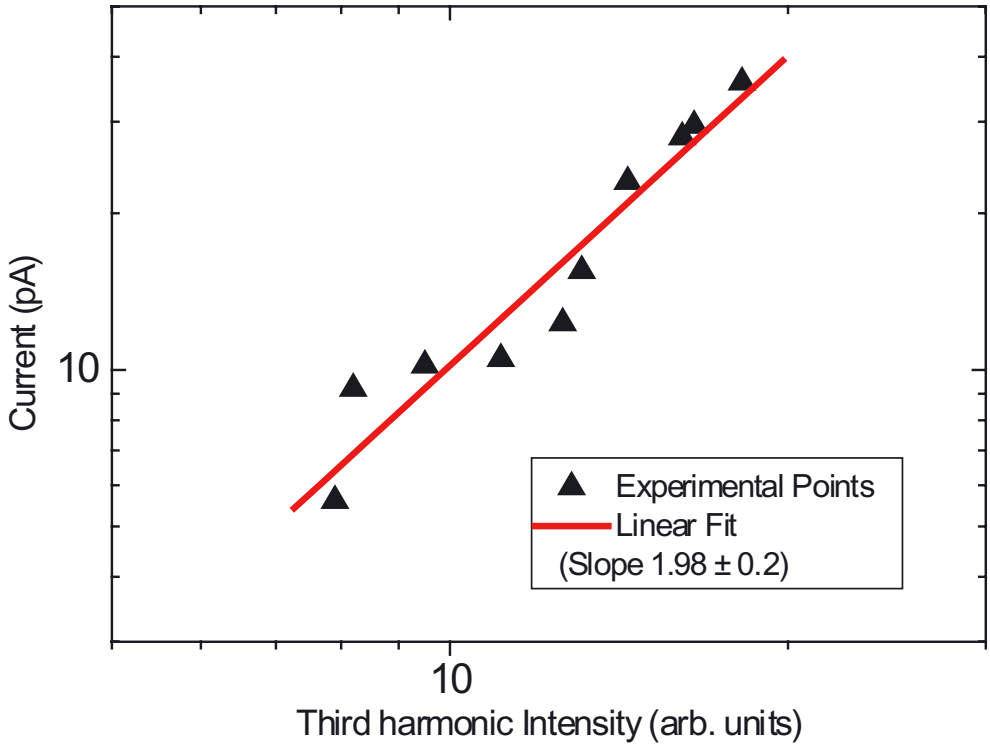

Figure 3.5: Two photon ionization yield, as a function of the intensity of the third harmonic.

3.2.6 Michelson UV interferometer

In order to confirm the results obtained by the grating interferometer, we utilized a conventional Michelson interferometer specially constructed for operation in the UV. This apparatus, utilizes a thin broadband beam splitter, as well as mirrors with high reflectivity and dispersion free operation in that spectral regime. Since both interferometers are operating in air, additional dispersion is always added to the propagating pulse either in the grating or in the Michelson interferometer. In order for the results obtained by both the interferometers to be comparable to each other, the Michelson optical paths a) where determined to be strictly equal with those of the grating interferometer and b)the thickness of the pellicle beam splitter is the same with that of the transmission grating i.e. 1 mm. Thus the overall dispersion introduced by both the interferometers is strictly the same. Additionally the delay unit, as well as the detection unit (toluene gas detector), are kept the same with those

used in the grating interferometer.

3.3 Experimental Results

3.3.1 Study of the spatial fringe profile

The ray tracing studies of the grating interferometer presented in chapter 2, indicated that tilting effects of the pulse-front, could somehow affect the spatial profile of the interference fringes, specially when the interferometer is utilized for the characteriza-

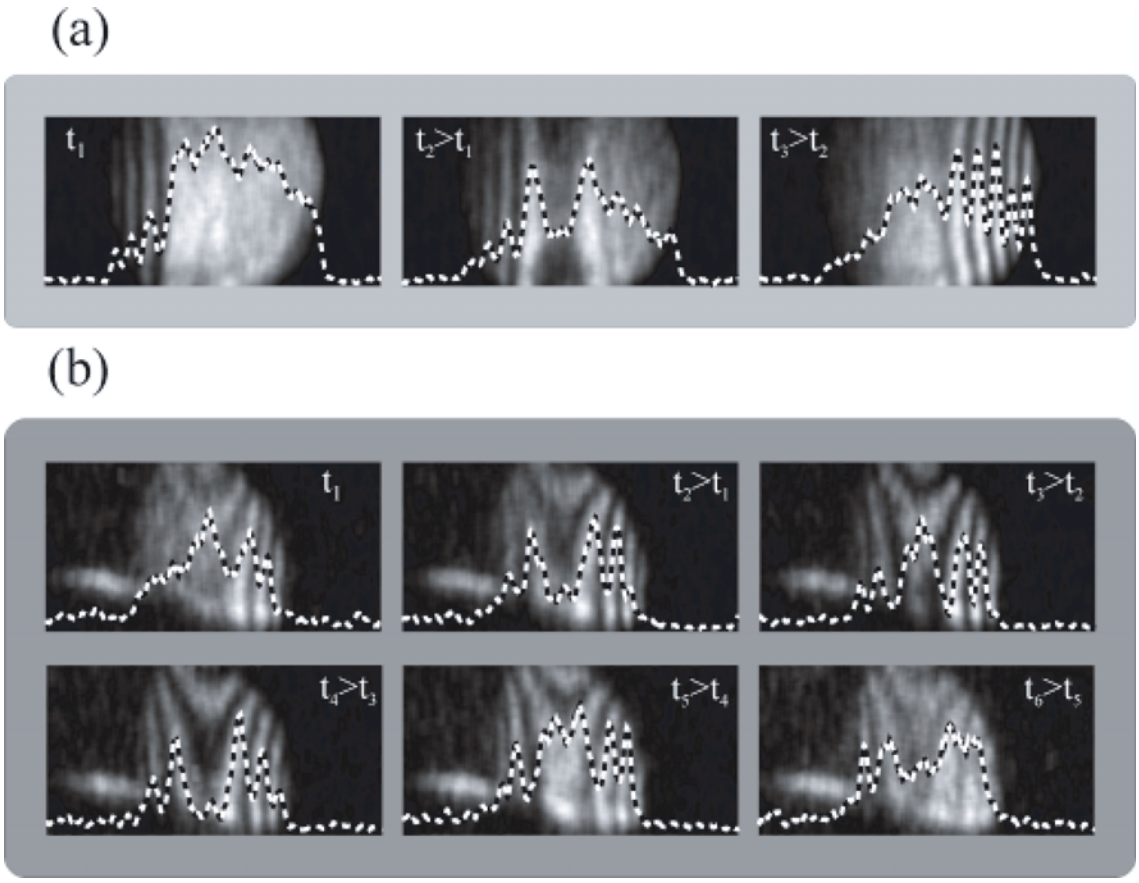

Figure 3.6: Spatial fringes of the two overlapping third harmonic pulses, recorded with the ICCD camera. **a.** before the MS3 **b.** After the MS3 mirror for different delays between the two pulses, originating from the two interferometer arms.

tion of lower harmonics. In order to investigate these effects an ICCD camera was employed. In Fig.3.6, the spatial fringes of the two overlapping third harmonic pulses

for different delays are depicted. The upper frame-set is taken before the Mirror MS3, see Fig.3.1 while the lower set corresponds to the spatial fringe profile, when the Case I geometry is implemented, i.e. the third mirror MS3 is properly positioned in order to image the grating to the detector plane (the ICCD plane for this study). Even if before the MS3, there is a continuous fringe moving from left to the right, after the MS3 the profile of the spatial fringes is stabilized, and only a variation of their contrast is observed as a function of the delay. This stabilization of the fringes indicates an additional contribution of the MS3 mirror in the improvement of the spatial fringes profile, and it is connected with the relative tilt reduction between the pulses corresponding to the two arms of the interferometer. A well stabilized fringe profile, is indispensable for the registration of higher order interferometric autocorrelation traces.

3.3.2 Single order interferometric autocorrelation

Once an interferometer is constructed, single order autocorrelation measurements are probably the most direct way to check the alignment and the validity of the interferometer, for high precision measurements. For the detection of signal, a linear photodiode was used. The interferometric trace obtained, is depicted in figure 3.7.a. In figure 3.7.b, the fourier transform of that trace is shown. The peak corresponds to the frequency of 3ω as expected and no other frequency with significant amplitude is indicated in the spectrum.

3.3.3 Second order interferometric autocorrelation

The utilization of toluene gas as a nonlinear detector according to the previous measurements, would allow the registration of second order autocorrelation traces, for both the Michelson and grating interferometer. The second order AC trace obtained

with the grating interferometer, is depicted in Fig. 3.8. The pulse duration is calculated to be 70 ±5 fs, assuming a gaussian temporal profile.

Similar traces are obtained, when the Michelson interferometer is used. The pressure in the toluene detector champer, is stabilized at the same value with the previous pulse measurements using the grating interferometer. A typical trace obtained by the Michelson interferometer is depicted in Fig.3.9. The pulse duration is calculated to be 65±5 fs.

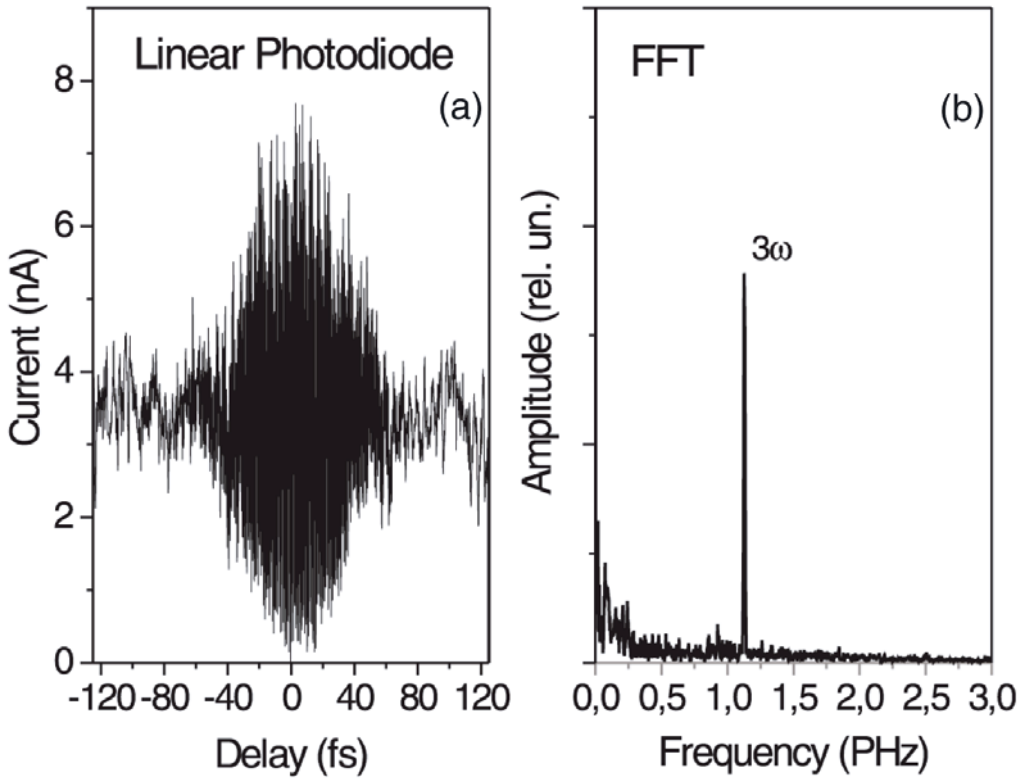

Figure 3.7: **a.** Single order autocorrelation trace of the third harmonic, on a linear photodiode. **b.** Fourier transform of the trace in **a**, where the peak indicates the frequency of the main oscillation corresponding to the third harmonic.

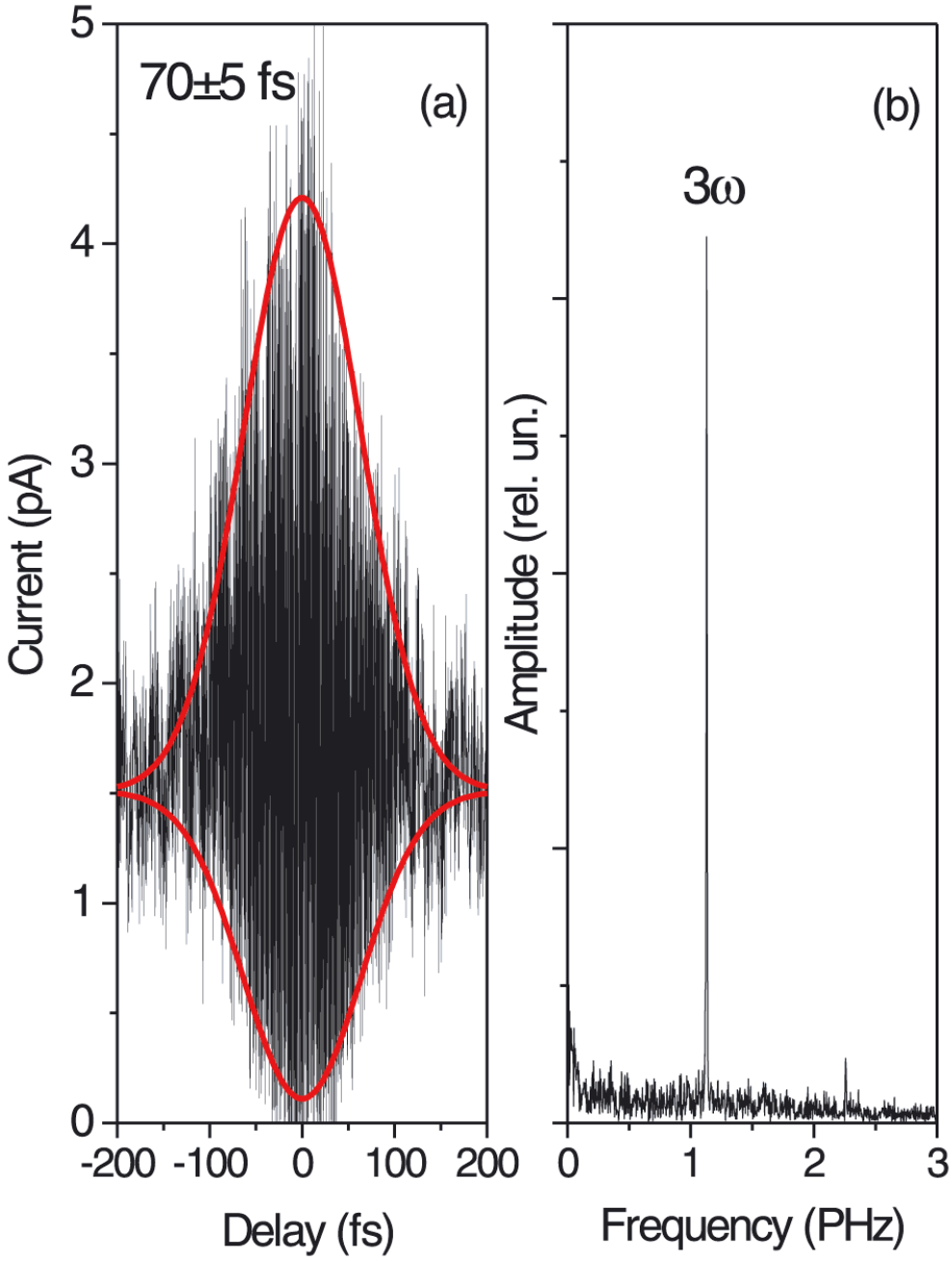

Figure 3.8: **a.** Second order interferometric AC trace obtained by the grating interferometer utilizing the toluene gas as a nonlinear detector. The red line is a guide for the eye. **b.** Fourier transform of the AC trace.

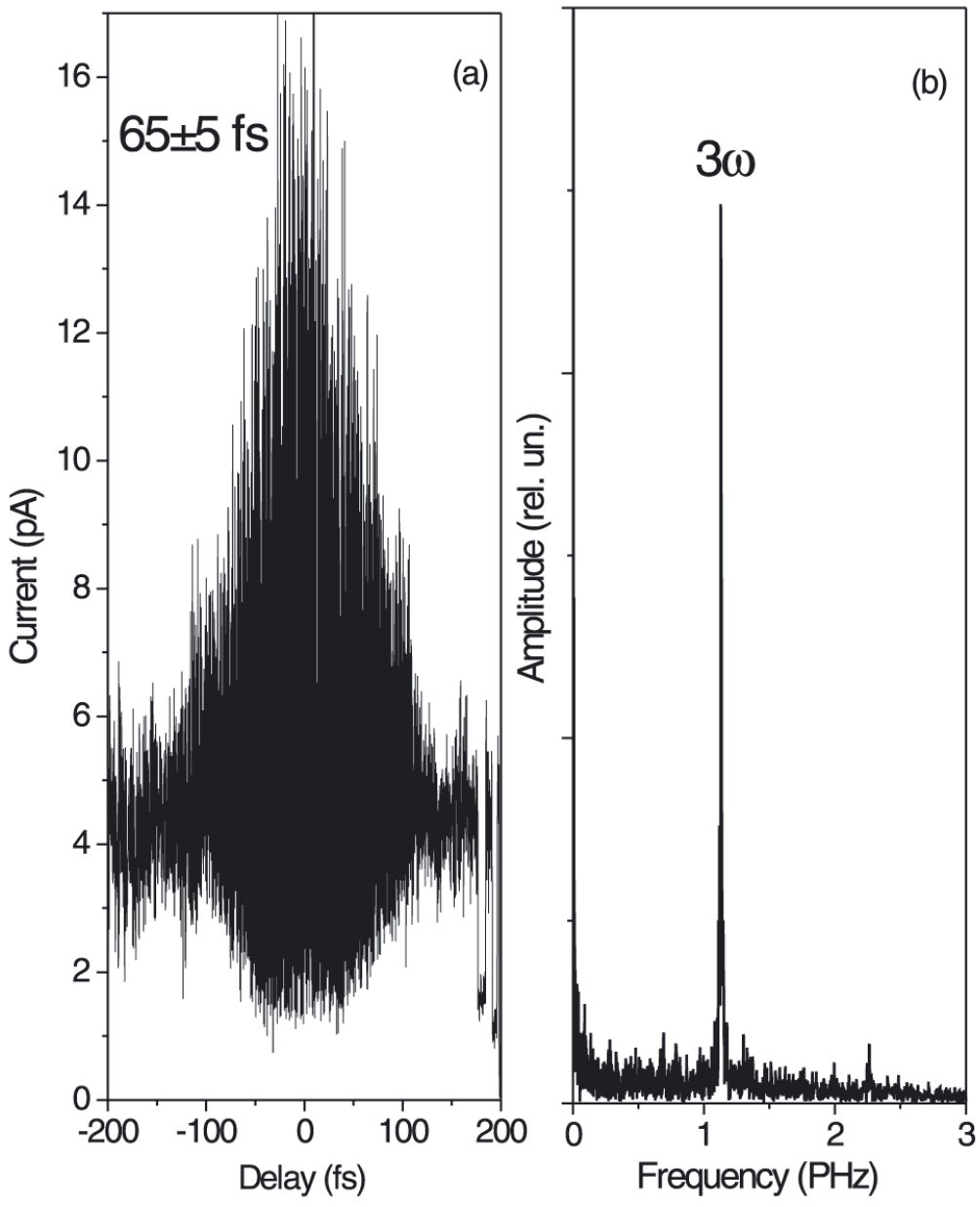

Figure 3.9: **a.** Second order interferometric AC trace obtained by the Michelson interferometer utilizing the toluene gas as a nonlinear detector. **b.** Fourier transform of the AC trace of a.

3.3.4 Third harmonic pulse propagation effects in toluene

In both pulse measurements presented, either with the Michelson or the grating interferometer, the pulse is measured to be much broader than expected by the lowest order perturbation theory. Their duration is even larger than the fundamental's. This can be attributed to the propagation of the pulse in the air and the rest dispersive materials i.e. transmission grating and beam splitter, that introduces chirp, resulting to a broadening of the pulse in to approximately the duration measured.

When the toluene gas pressure in the detection cell is varied, several interesting effects connected with the measured third harmonic pulse duration are taking place. In order to investigate these effects we perform a series of intensity autocorrelation measurement, scanning a wide range of the toluene pressure. A typical intensity autocorrelation of the third harmonic pulse is depicted in Fig.3.10. Figure 3.11 depicts the pulse duration measured as a function of the toluene pressure in the detector cell. The minimum pulse duration (25 fs) in a pressure of 4 mbar corresponds within the experimental error to that expected by the lowest order perturbation theory since the fundamental has a duration of 45 fs. These effects can be attributed to possible pulse recompression by the toluene gas when used under the above described experimental conditions. A well known issue from the fundamental theory of optics is that negative dispersion can be possessed by material when the propagating radiation is spectrally located near to an absorption resonance. Since most of the spectral lines of the materials are located in the UV, this behavior is not observed when infrared or visible light pulse are interact with them. In the case of UV pulses specially when they are spectrally located near a material's resonance negative dispersion can be observed. In particular for gaseous media, these effects are expected to be pressure depended since the index of refraction is density depended as well. On light of the above consideration, keeping the toluene cell in low pressure values the negative GDD introduced is quite low for pulse compensation. After an optimum density value where

the pulse is re-compensated to it's fourier transform limited duration, the duration starts to increase again up to 65-70 fs as a result of the dispersion introduced by the toluene gas itself. Nevertheless a full understanding to the propagation effects would require additional information concerning the complex index of refraction as well as the role of the toluene's ionization in that spectral regime and unfortunately this information has not been accessed so far.

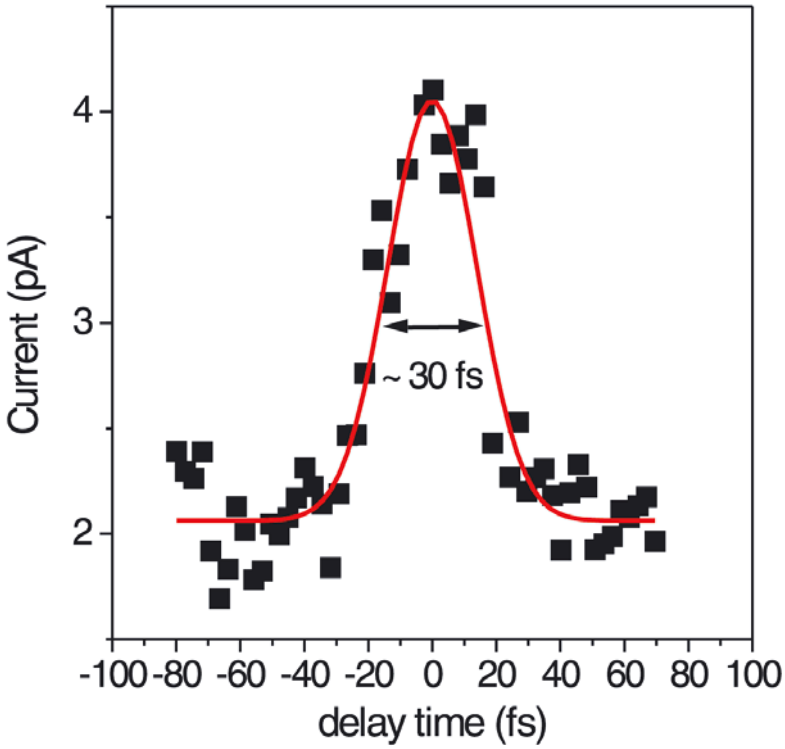

Figure 3.10: Intensity autocorrelation of the third harmonic, with the toluene pressure at 3 mbar. The red line, corresponds to a gaussian fit on the experimental data resulting to a pulse duration of 30 fs.

3.3.5 Discussion on the results

As already mentioned the pulse duration measured under identical conditions by the two interferometer is the same within the accuracy of the measurement i.e. $\sim$ 67

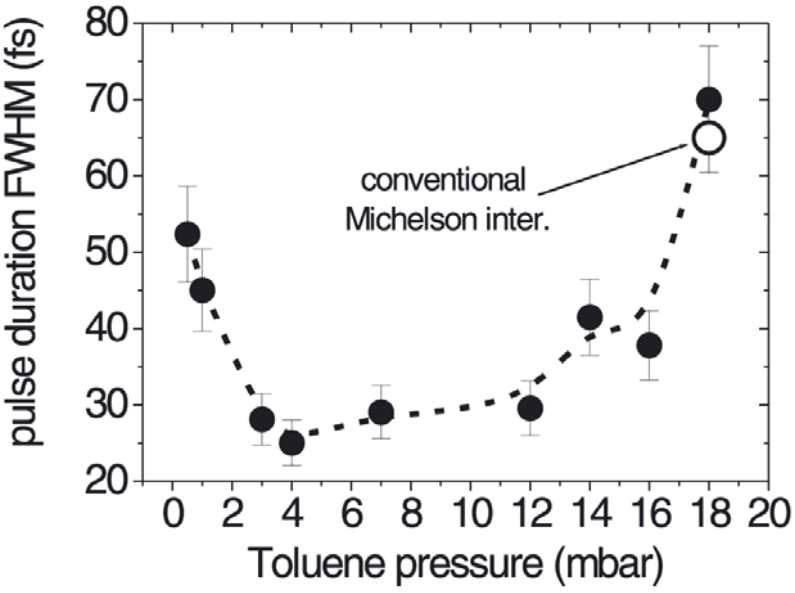

Figure 3.11: Measured third harmonic pulse duration, as a function of the Toluene pressure in the detection cell when the grating interferometer is used. The open cycle, represents the comparative measurement with the Michelson interferometer.

fs. The interferometric autocorrelation traces presented exhibit a deviation from the 8:1 peak to background ratio and the intensity trace from 3:1 ratio. There are several reasons that may contribute to that deviation. The surface quality of the spherical mirrors ($\lambda/3$ $\lambda/2$ for 267 nm) prevent a perfect beam profile. Additionally, the imperfect balance of energy between the two interferometer arms the slight tilt between the pulse fronts of the interferometer arms and the single photon contribution of the intermediate resonance of toluene at (267 nm) which add additional background are also contribute to the decrease of the peak to background ratio.

To our knowledge these are the first nonlinear interferometric autocorrelation traces of a harmonic pulse produced in gaseous medium ever measured. Therefore together with its high stability, the spectral selectivity and the uniform energy distribution on it's arms it can be concluded that the grating interferometer can serve as an appropriate system for the temporal characterization of harmonics.

Conclusions and outlook

In conclusion, we proposed and analyzed a novel application of a transmission grating utilized as a beam splitter, and we developed a Michelson interferometer appropriate for temporal studies in the UV-XUV spectral regime. By examining three different geometries of the interferometer using ray tracing simulations we concluded that they posses extremely low dispersion characteristics and found them suitable for implementing single or higher order interferometric autocorrelations for a single harmonic or harmonic superpositions, in the XUV spectral region. Additionally, a version of the interferometer which combines low dispersion and tide harmonic focusing was found to be appropriate for the implementation of cross correlation techniques in the UV-XUV region. Further, an experimental demonstration of the grating interferometer for retrieving the temporal characteristics of the third harmonic of a Ti:Saph laser, was performed. The interferometer was studied in detail and a second order interferometric autocorrelation of the third harmonic produced on argon gas was obtained by utilizing the gaseous toluene as a nonlinear detector. Comparative measurements using a conventional Michelson interferometer were found to be in excellent agreement with those of the grating interferometer confirming its suitability for high precision measurements. A future perspective would be the use of the interferometer for the characterization of higher harmonics and this would require the use of the experimental setup in vacuum either for its autocorrelation versions Case I, Case II or of the cross correlation configuration Case III. Additionally the proper nonlinear detection

unit has to be found and evaluated. According to the estimations presented in chapter 2 as well as the experiments carried out so far it is suggested that the single or double ionization of noble gasses would be a possible nonlinear process for registering a well observable two photon signal in the XUV. Together with its accurate spectral selectivity, and its relative easy alignment since a lower harmonic is involved as guide for aligning the invisible XUV, the interferometer could strongly contribute to the full measurement of the temporal characteristics of harmonics as well of attosecond pulses which are probably the most promising route for implementing the next generation light sources appropriate for the investigation of the temporal dynamics of matter at the atomic scale.

References

Antoine P., A. L'Huillier, and M. Lewenstein, *Phys. Rev. Lett.* **77**, 1234 (1996).

Backus S., J. Peatross, Z. Zeek, A. Rundquist, G. Taft, M. M. Murnane, and H.C.Kapteyn, *Optics Lett.*, **21**, 665 (1996).

Bräuninger H., P. Predehl, and K. P. Beuermann, App. *Optics* **18**, 368 (1979).

Christov I. P., M. M. Murnane, and H. C. Kapteyn, *Phys. Rev. Lett.* **78**, 1251 (1997).

Constant E., D. Garzella, P. Breger, E. Mevel, Ch. Dorrer, C. Le Blanc, F. Salin, and P. Agostini, *Phys. Rev. Lett.* **82**, 1668, (1999).

Corkum P.B., N.H.Burnett, and M.Y.Ivanov, *Opt. Lett.*, **19**, 22, (1994).

Corkum P.B., *Phys. Rev. Lett.*,**71**, 1994, (1993).

Dadap J. I., G. B. Focht, D.H. Reitze, and M.C. Downer, *Opt. Lett.***16**, 499, (1991)

Drescher M., M. Hentschel, R. Kienberger, G. Tempea, C. Spielmann, G. A. Reider, P. B. Corkum, and F. Krausz, *Science* **291**, 1923 (2001).

Eidmann K., M. Kühne, P. Müller, and G. D. Tsakiris, *J. of X-ray Science and Tech.* **2**, 259 (1990).

Farkas Gy. and Cs. Toth, *Phys. Lett. A* **168**, 447 (1992).

Goulielmakis E., *Diploma thesis*, (2000), unpublished.

Hentschel M., R. Kienberger, Ch. Spielmann, G. A. Reider, N. Milosevic, T. Brabec, P. Corcum, U. Heinzmann, M. Drescher, *Nature* **414**, 509 (2001).

Hergott J. F., M. Kovacev, H. Merdji, C. Hubert, Y. Mairesse, E. Jean, P. Agostini, B. Carre and P. Salieres, *private communication* (2002).

Kobayashi Y., T. Sekikawa, Y. Nabekawa, S. Watanabe, *Opt. Lett.* **23**, 64 (1998).

L Huillier A., M. Lewenstein, P. Salieres, Ph. Balcou, M. Yu. Ivanov, J. Larsson, and C. G. Wahlström, *Phys. Rev. A*, **48**, R3433 (1993).

Lochbihler H. and R. A. Depine, *Opt. Comm.* **100**, 231 (1993).

Macklin J. J., J. D. Kmetec and C. L. Gordon III, *Phys. Rev. Lett.* **70**, 766 (1993).

Norin J., J. Mauritsson, A. Johansson, M. K. Raarup , S. Buil, A. Persson, O. Dhr, M. B. Gaarde, K. J. Schafer, U. Keller, C. G. Wahlström, and A. LHuillier, *Phys. Rev. Lett.* **19**, 88 (2002).

Papadogiannis N. A., to be published, (2002).

Papadogiannis N. A., B. Witzel, C. Kalpouzos, and D. Charalambidis, *Phys. Rev. Lett.* **83**, 4289 (1999).

Papadogiannis N. A., C. Kalpouzos, B. Witzel , C. Fotakis, D Charalambidis *J. Phys. B.* **33**, L79, (2000).

Papadogiannis N. A., C. Kalpouzos, E. Goulielmakis, G. Nersisyan, D. Charalambidis, F. Auge, F. Weihe, and Ph. Balcou, *Appl. Phys. B* **73** (2002).

Paul P. M., E. S. Toma, P. Breger, G. Mullot, F. Auge, Ph. Balcou, H. G. Muller, and P. Agostini, *Science* **292**, 1689 (2001).

Ronchi Vasco, App. *Optics* **3**, 437 (1963).

Sala K. L., G. A. Kenney-Wallace, and G. E. Hall, *J. of quantum electronics* **QE-16**, 990 (1980).

Schnurer M., Ch. Spielmann, P. Wobrauschek, C. Streli, N. H. Burnett, C. Kan, K. Fenencz, R. Koppitsch, Z. Cheng, T. Brabec, F. Krausz *Phys. Rev. Lett.* **80**, 3236 (1998).

Sekikawa T., T. Ohno, T. Yamazaki, Y. Nabkawa, and S.Watanabe. *Phys. Rev. Lett.* **83**, 2564 (1999).

Siders C. W., N. C Turner III, M. C. Downer, A. Babine, A. Stepanov, and A. M. Sergeev, *J. Opt. Soc. Am.* **13**, 330 (1996).

Siegman A.E., Lasers, University Science Books, Mill Valley, CA, 1986..

Spielmann Ch., N. H. Burnett, S. Sartania, R. Koppitsch, M. Schnurer, C. Kan, M. Lenzner, P. Wobrauschek, and F. Krausz, *Science*, **278**, 661, (1997).

Streltsov A. M., J. K. Ranka, and A. L. Gaeta, *Opt. Lett.* **23**, 798 (1998).

Toma E. S., H. G. Muller, P. M. Paul, P. Breger, M. Cheret, P. Agostini, C. Le Blanc, G. Mullot and G. Cheriaux, *Phys. Rev. A*, **62**, 061801 (2000).

Treacy E. B., *IEEE J of Quan. Elec.* **QE-5**, 454 (1969).

Xenakis D., O. Faucher, D. Charalambidis, and C. Fotakis, *J. Phys. B*, **29**, L457 (1996).

Zhou J., J. Peatross, M. M. Murnane, H. C. Kapteyn, and I. P. Christov. *Phys. Rev. Lett.* **76**, 752 (1996).

Acknowledgements

I would like to thank Professor Dimitrios Charalambidis for his support, his encouragement and for giving me the opportunity to work with him and his group in this interesting scientific field.

Also I would like to thank Dr. Giorgos Tsakiris for the perfect collaboration that we had during the calculations and the experimental work presented in this thesis.

Dr. Nektarios Papadogiannis in the beginning and Dr. Gagik Nersisyan later, were the people that helped me to understand how thinks work in a scientific lab.

Finally, I would like to thank Professor Costas Fotakis for his support, during my studentship in IESL -FORTH.